nature genetics

ARTICLES

https://doi.org/10.1038/s41588-018-0120-1

Analysis of the androgen receptor–regulated lncRNA landscape identifies a role for ARLNC1 in prostate cancer progression

Yajia Zhang[1,2,3,4,23], Sethuramasundaram Pitchiaya[1,2,23], Marcin Cieślik[1,2,23], Yashar S. Niknafs[1,5], Jean C.-Y. Tien[1,2], Yasuyuki Hosono[1], Matthew K. Iyer[1,4], Sahr Yazdani[1], Shruthi Subramaniam[1], Sudhanshu K. Shukla[1,20], Xia Jiang[1], Lisha Wang[1], Tzu-Ying Liu[6], Michael Uhl[7], Alexander R. Gawronski[8], Yuanyuan Qiao[1,2,9], Lanbo Xiao[1], Saravana M. Dhanasekaran[1,2], Kristin M. Juckette[1], Lakshmi P. Kunju[1,2,9], Xuhong Cao[1,10], Utsav Patel[11], Mona Batish[11,12], Girish C. Shukla[13], Michelle T. Paulsen[9,14], Mats Ljungman[9,14], Hui Jiang[6,9], Rohit Mehra[2,9,15], Rolf Backofen[7], Cenk S. Sahinalp[16,17], Susan M. Freier[18], Andrew T. Watt[18], Shuling Guo[18], John T. Wei[15], Felix Y. Feng[1,9,14,19,21], Rohit Malik[1,22,24] and Arul M. Chinnaiyan[1,2,4,5,9,10,15,24]*

The androgen receptor (AR) plays a critical role in the development of the normal prostate as well as prostate cancer. Using an integrative transcriptomic analysis of prostate cancer cell lines and tissues, we identified ARLNC1 (AR-regulated long noncoding RNA 1) as an important long noncoding RNA that is strongly associated with AR signaling in prostate cancer progression. Not only was ARLNC1 induced by the AR protein, but ARLNC1 stabilized the *AR* transcript via RNA–RNA interaction. ARLNC1 knockdown suppressed AR expression, global AR signaling and prostate cancer growth in vitro and in vivo. Taken together, these data support a role for ARLNC1 in maintaining a positive feedback loop that potentiates AR signaling during prostate cancer progression and identify ARLNC1 as a novel therapeutic target.

Long noncoding RNAs (lncRNAs) are a class of transcripts with diverse and largely uncharacterized biological functions[1–3]. Through crosstalk with chromatin, DNA, RNA species and proteins, lncRNAs function via chromatin remodeling, as well as transcriptional and post-transcriptional regulation[4–9]. High-throughput RNA sequencing (RNA-seq) has enabled the identification of lncRNAs with suggested oncogenic and tumor-suppressive roles, including involvement in the pathogenesis of prostate cancer[7,10–12]. Primary prostate cancer is often hormone dependent and relies on signaling through the AR; therefore, the majority of patients are responsive to front-line treatment with androgen-deprivation therapy[13–15]. However, approximately 20% of cases progress to an incurable stage of the disease known as castration-resistant prostate cancer (CRPC), which still critically relies on AR signaling[16,17], as evidenced by the clinical benefit afforded through the use of enzalutamide[18–21] or abiraterone[22–24]. While substantial efforts have been undertaken to identify mechanisms of sustained AR signaling in CRPC (i.e., AR alterations, *AR* splice variants and alternative activation pathways)[25–31], few studies have investigated the role of AR-regulated lncRNAs. Therefore, we initiated a comprehensive RNA-seq profiling investigation of AR-regulated, cancer-associated lncRNAs from prostate cancer cell lines and patient tissue samples.

Results

Analysis of AR-regulated transcriptome in prostate cancer. To nominate AR-regulated genes (ARGs), RNA-seq was performed on AR-dependent VCaP and LNCaP prostate cancer cell lines that were stimulated with an AR ligand, dihydrotestosterone (DHT), for 6 and

[1]Michigan Center for Translational Pathology, University of Michigan, Ann Arbor, MI, USA. [2]Department of Pathology, University of Michigan, Ann Arbor, MI, USA. [3]Molecular and Cellular Pathology Program, University of Michigan, Ann Arbor, MI, USA. [4]Department of Computational Medicine and Bioinformatics, Ann Arbor, MI, USA. [5]Department of Cellular and Molecular Biology, University of Michigan, Ann Arbor, MI, USA. [6]Department of Biostatistics, University of Michigan, Ann Arbor, MI, USA. [7]Department of Computer Science and Centre for Biological Signaling Studies (BIOSS), University of Freiburg, Freiburg, Germany. [8]School of Computing Science, Simon Fraser University, Burnaby, British Columbia, Canada. [9]Rogel Cancer Center, University of Michigan, Ann Arbor, MI, USA. [10]Howard Hughes Medical Institute, University of Michigan, Ann Arbor, MI, USA. [11]New Jersey Medical School, Rutgers University, Newark, NJ, USA. [12]Department of Medical Laboratory Sciences, University of Delaware, Newark, DE, USA. [13]Department of Biological, Geological and Environmental Sciences, Center for Gene Regulation in Health and Disease, Cleveland State Univesity, Cleveland, OH, USA. [14]Department of Radiation Oncology, University of Michigan, Ann Arbor, MI, USA. [15]Department of Urology, University of Michigan, Ann Arbor, MI, USA. [16]School of Informatics and Computing, Indiana University, Bloomington, IN, USA. [17]Vancouver Prostate Centre, Vancouver, British Columbia, Canada. [18]Ionis Pharmaceuticals, Carlsbad, CA, USA. [19]Breast Oncology Program, University of Michigan, Ann Arbor, MI, USA. Present address: [20]Department of Biosciences and Bioengineering, Indian Institute of Technology Dharwad, Dharwad, India. [21]Departments of Radiation Oncology, Urology, and Medicine, Helen Diller Family Comprehensive Cancer Center, University of California at San Francisco, San Francisco, CA, USA. [22]Bristol-Myers Squibb, Princeton, NJ, USA. [23]These authors contributed equally: Yajia Zhang, Sethuramasundaram Pitchiaya, Marcin Cieślik. [24]These authors jointly supervised this work: Rohit Malik, Arul M. Chinnaiyan. *e-mail: arul@umich.edu

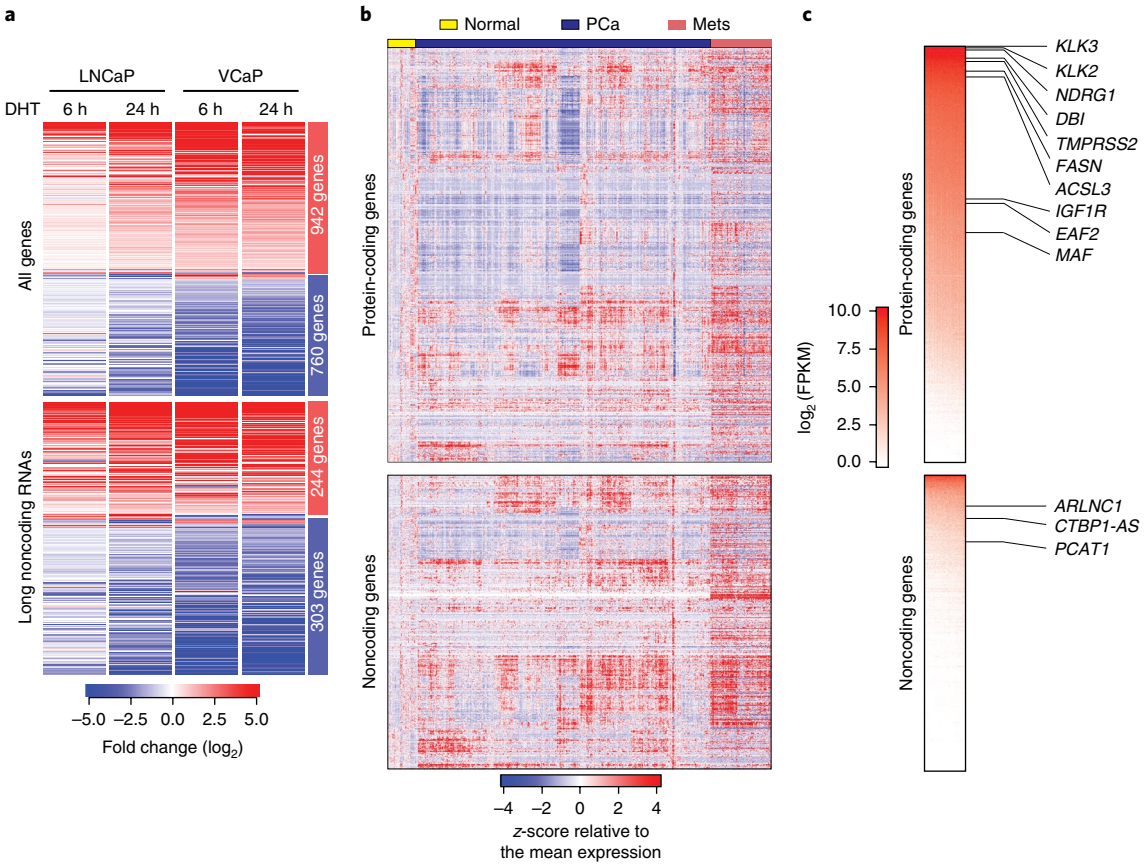

Fig. 1 | Identification of AR-regulated genes in prostate cancer. a, The androgen-regulated transcriptome of prostate cancer cells. The heat map represents the 1,702 genes (including 547 lncRNAs) differentially regulated in LNCaP and VCaP cells following 6 and 24 h of DHT treatment. **b**, The landscape of transcriptomic alterations of prostate cancer progression. The heat map depicts 1,155 protein-coding genes and 547 lncRNAs across benign prostate (normal, $n=52$ samples), localized prostate cancer (PCa, $n=500$ samples) and metastatic prostate cancer (Mets, $n=100$ samples) in TCGA prostate and SU2C-PCF RNA-seq data, with rows representing genes and columns representing patients. Patients were grouped by clinical stage, and genes were subjected to hierarchical clustering. Expression variability is quantified for each gene as a *z*-score relative to the mean expression in normal prostate samples. **c**, A heat map representation of ranked median gene expression levels in prostate tissues. Canonical prostate lineage and prostate cancer markers are listed.

24 h (Supplementary Fig. 1a). A total of 1,702 genes were identified to be concordantly induced or repressed in VCaP and LNCaP cells at both time points (Fig. 1a, Supplementary Fig. 1b,c and Supplementary Table 1), including more than 500 lncRNAs (Fig. 1a and Supplementary Fig. 1d); these data indicate that a large portion of the AR transcriptome remains uncharacterized.

To differentiate between direct and indirect ARGs, previously published and in-house AR chromatin immunoprecipitation (ChIP)–seq data from LNCaP and VCaP cells were analyzed[32]. As expected for direct AR targets, increased levels of AR binding at transcription start sites (TSSs) in both LNCaP and VCaP cells were observed (Supplementary Fig. 1e). The binding levels decreased following treatment with an AR antagonist (enzalutamide) (Supplementary Fig. 1f,g), and the binding sites revealed a de novo motif identical to the canonical AR response element[33] (Supplementary Fig. 1h). A total of 987 genes were categorized as direct ARGs, including 341 lncRNAs (lncARGs) (Supplementary Table 1). Within these genes, we observed an enrichment of chromatin marks associated with 'open' chromatin (H3K27ac, H3K4me1), active promoters (H3K4me3) and transcription (H3K36me3), which, together with RNA polymerase II (Pol II) occupancy, are recognized as manifestations of active gene expression (Supplementary Fig. 1i). Bromodomain and extra-terminal (BET) family proteins, such as BRD4, recognize acetylated histones and have been shown to promote AR transcriptional activity[32]. Consistent with this, we observed colocalization of BRD4 and AR proteins at the promoters of direct AR-responsive genes and loss of AR ChIP peaks following treatment with a bromodomain inhibitor (JQ1) (Supplementary Fig. 1f,i). We further sought to determine whether ARGs identified from cell lines were also targeted by AR in normal prostate tissues and primary tumors. We leveraged a published dataset[34] and queried for the presence of AR peaks within ARG promoters. Remarkably, the majority of ARG promoters were TSS-proximally bound by AR in both tissues and cell lines (Supplementary Fig. 1j,k); conversely, AR-independent genes were distal to AR-binding sites (Supplementary Fig. 1l).

Finally, we confirmed that the ARGs were also expressed in human prostate tissues. We interrogated RNA-seq data from normal prostate, clinically localized prostate cancer (The Cancer Genome Atlas, TCGA)[35] and metastatic CRPC (Stand Up to Cancer–Prostate Cancer Foundation, SU2C-PCF)[30] (Fig. 1b). This revealed remarkable heterogeneity in the expression of ARGs during prostate cancer progression to metastatic disease. As expected, compared to protein-coding genes, noncoding ARGs were detected at lower overall levels (Fig. 1c), although ~10% showed robust expression of over 10 FPKM (fragments per kilobase of transcript per million mapped reads) on average across prostate cancer samples.

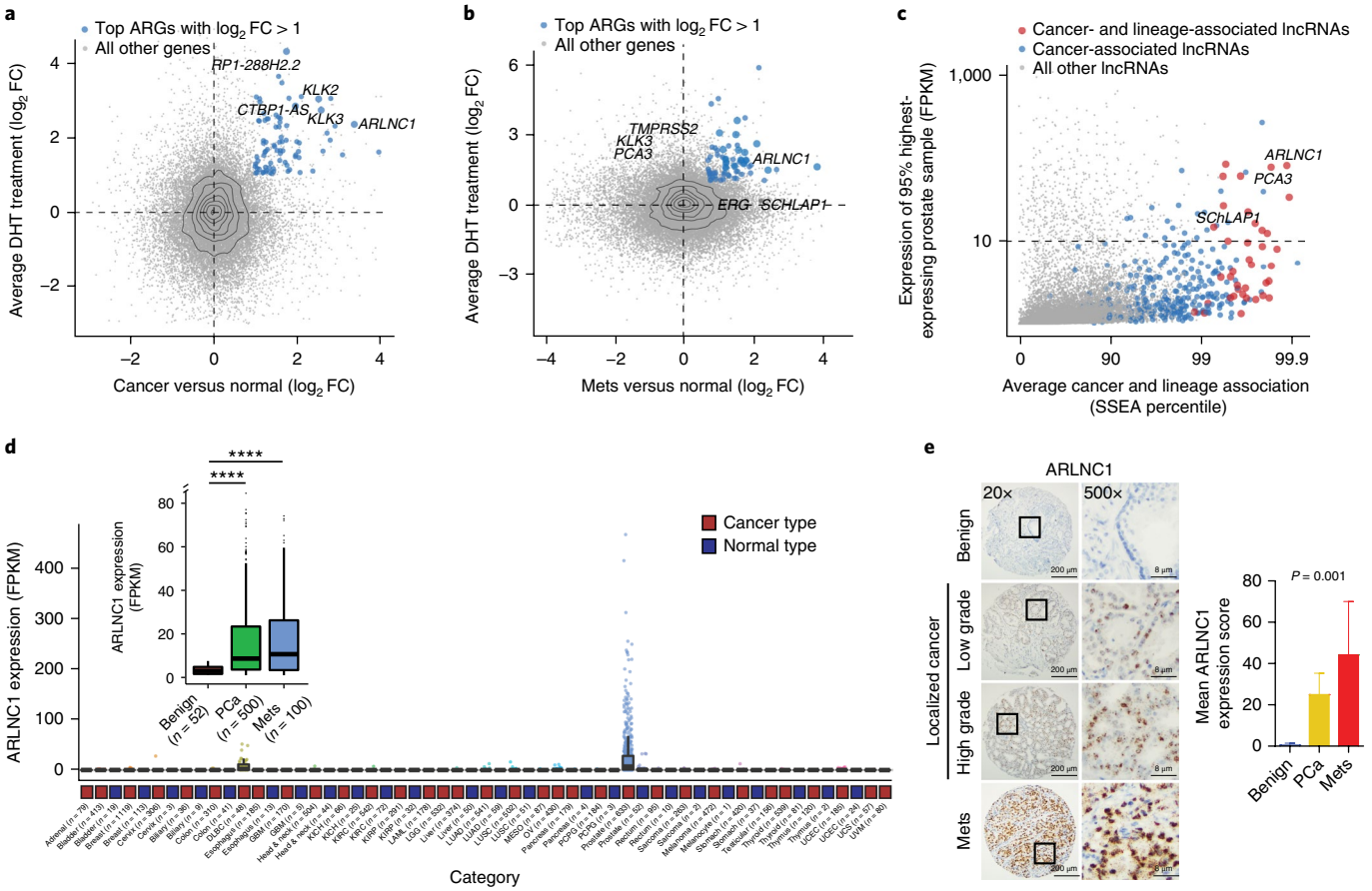

Fig. 2 | Nomination and in situ characterization of ARLNC1 in prostate cancer. a,**b**, Identification of androgen-regulated transcripts elevated in prostate cancer progression. Scatterplots show the AR regulation and cancer association of the ARGs identified in Fig. 1a. The *y* axis depicts the $\log_2$-transformed fold change in gene expression following DHT stimulation, and the *x* axis indicates the $\log_2$-transformed difference in gene expression level between benign prostate ($n=52$ samples) and localized prostate cancer ($n=500$ samples) (**a**) and between benign prostate ($n=52$ samples) and metastatic prostate cancer ($n=100$ samples) (**b**). Significant genes with $\log_2$ fold change > 1 were ranked according to combined *P* value (limma-moderated *t* test). **c**, Nomination of prostate cancer- and lineage-associated lncRNAs based on expression levels. The scatterplot shows the expression level, prostate tissue specificity and prostate cancer association of lncRNAs. The expression level is the FPKM value at the 95th percentile across TCGA prostate samples. Average cancer and lineage associations are represented by the percentile rank for each gene in SSEA (total $n = 7{,}256$ samples). **d**, Relative expression (FPKM) of ARLNC1 across different cancer types in the TCGA cohort. Inset, relative expression (FPKM) of ARLNC1 across benign prostate ($n=52$ samples), localized prostate cancer ($n=500$ samples) and metastatic prostate cancer ($n=100$ samples). PCa versus Normal: $^{****}P < 2.2\times10^{-16}$; Mets versus Normal: $^{****}P = 2.6\times10^{-7}$ (two-sided *t* test). Box-plot definitions: the center line depicts the median, the box shows the first and third quartiles, and the whiskers follow the 1.5 rule. **e**, ISH of ARLNC1 transcript in a human prostate cancer tissue microarray. Representative ARLNC1 staining is shown for benign prostate and localized and metastatic prostate cancer tissue. The bar plot represents mean ARLNC1 expression scores across benign prostate ($n=11$), localized prostate cancer ($n=85$) and metastatic prostate cancer ($n=37$) tissues, with vertical bars indicating the bootstrapped 95% confidence interval of the means. Significance was calculated by a Kruskal–Wallis rank-sum test.

ARLNC1 is a prostate lineage-specific lncRNA with elevated expression in cancer. We hypothesized that lncRNAs associated with prostate cancer progression and castration resistance should be either upregulated if they enhance AR signaling or, conversely, downregulated if they attenuate AR signaling. Their expression is also expected to be AR dependent and lineage restricted if they are part of bona fide physiological feedback loops. Accordingly, a top–down strategy was developed to establish and prioritize clinically relevant, prostate cancer- and lineage-specific lncARGs. First, we identified genes that were both regulated by AR in the VCaP and LNCaP cell lines and upregulated in primary (Fig. 2a) or metastatic (Fig. 2b) prostate cancer as compared to normal prostate tissues. As expected, canonical AR targets, including *KLK3*, *KLK2* and *TMPRSS2*, were among the most differentially expressed protein-coding genes. Notably, this approach highlighted several novel lncARGs, including *ARLNC1* (*ENSG00000260896*, *PRCAT47*[10]), and validated previously identified lncARGs, such as *CTBP1-AS*[36] (Fig. 2a,b). Interestingly, *ARLNC1* was found to be one of the most differentially expressed AR-regulated genes in both localized and metastatic prostate cancer (Fig. 2a,b and Supplementary Fig. 2a,b).

Next, we sought to establish the prostate lineage and cancer specificity of prostate cancer–associated lncRNAs. We leveraged the MiTranscriptome assembly[10], an online resource, to interrogate lncRNA expression across a multitude of tissue and tumor types, and we calculated sample set enrichment analysis (SSEA) scores, which indicate the strength of cancer and lineage association[10]. After applying an expression-level filter (10 FPKM at the 95th percentile), we identified 12 of the most prostate lineage- and cancer-specific lncRNAs (Fig. 2c and Supplementary Fig. 2c,d); 5 of these lncRNAs were regulated by AR. Across these analyses, ARLNC1 was the top prioritized transcript and thus warranted further investigation.

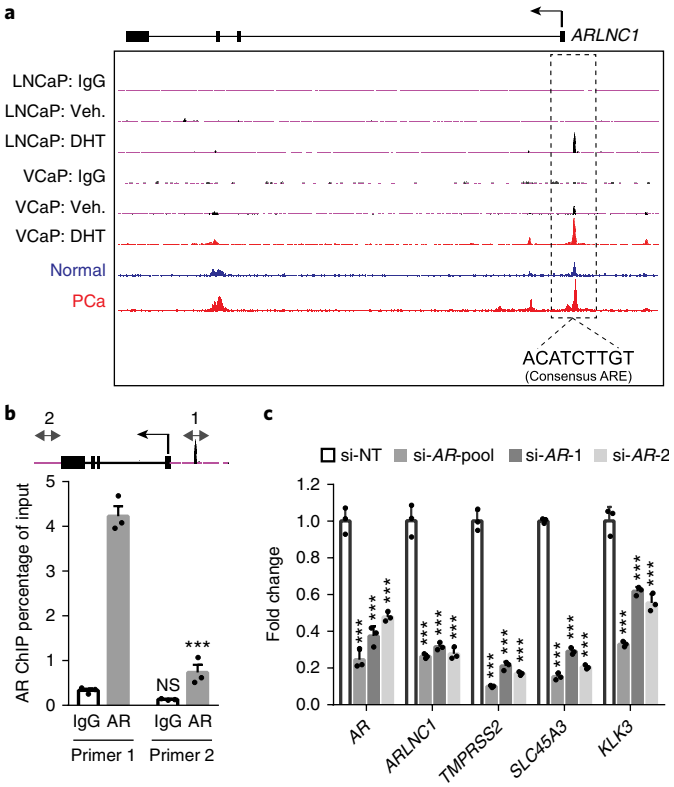

Fig. 3 | *ARLNC1* is directly regulated by AR. a, AR ChIP–seq in prostate cancer cell lines and tissues. Normalized ChIP–seq enrichment is shown. Top, AR or control (IgG) ChIP–seq results across the *ARLNC1* locus in LNCaP and VCaP cells with vehicle (ethanol) or DHT treatment. Bottom, AR ChIP–seq in benign prostate and clinically localized prostate cancer tissue. ARE, androgen response element. **b**, ChIP–qPCR in MDA-PCa-2b cells showing AR or IgG enrichment (ChIP/input) over the *ARLNC1* promoter region (primer 1) or a control region (primer 2). Data are shown as the mean ± s.e.m. ($n = 3$ biologically independent samples). ***P (adjusted) < 0.0001, NS (not significant): $P = 0.5746$, compared to the control region (primer 2) by ANOVA with Sidak correction for multiple comparisons. Top, schematic of the amplicon locations for ChIP–qPCR validation. **c**, Expression of *AR* and AR target genes (*ARLNC1*, *TMPRSS2*, *SLC45A3* and *KLK3*) in MDA-PCa-2b cells transfected with control siRNA (si-NT) or siRNAs against *AR* (si-*AR*-pool, si-*AR*-1, si-*AR*-2). Mean ± s.e.m. values are shown, $n = 3$ biologically independent samples. ***$P = 0.0001$, determined by ANOVA with Dunnett's multiple-comparisons test.

Expression of ARLNC1 was interrogated across cancer and normal tissue RNA-seq samples from TCGA and the Genotype-Tissue Expression (GTEx) project[37,38], respectively. In the TCGA cohort, ARLNC1 exhibited a highly prostate cancer–specific expression pattern, with little to no expression in other tumor types (Fig. 2d). Similarly, in the GTEx normal tissue cohort, its expression was limited to the prostate (Supplementary Fig. 2e). Among the prostate samples, ARLNC1 expression was significantly higher in localized and metastatic prostate cancers than in benign tissues, as assessed by RNA-seq (Fig. 2d, inset) and in situ hybridization (ISH; Fig. 2e). In an extensive differential expression analysis using MiTranscriptome, ARLNC1 was found to be among the top 1% of transcripts most upregulated in prostate cancer and specific to the prostate lineage, with no significant associations in other tissues (Supplementary Fig. 2f). Moreover, the protein-coding genes that were most correlated with ARLNC1 were found to be associated with prostate cancer progression in ONCOMINE concept analyses performed on multiple clinical datasets[39] (Supplementary Fig. 2g). Together, these results confirm that ARLNC1 expression is restricted to the prostate lineage, elevated in prostate cancer and associated with AR signaling throughout prostate cancer progression.

To functionally characterize ARLNC1, we first identified appropriate prostate cancer cell lines with moderate to high levels of ARLNC1 expression using in-house RNA-seq data (Supplementary Fig. 3a). Supporting the association of AR with ARLNC1, ARLNC1 expression was highly enriched in AR-positive cell lines, with the highest expression in MDA-PCa-2b and LNCaP cells. In addition, qPCR analysis for the ARLNC1 transcript also demonstrated that this gene was expressed at the highest level in the MDA-PCa-2b and LNCaP cell lines (Supplementary Fig. 3b). As existing annotations of the *ARLNC1* gene (located on chromosome 16) predict the presence of several transcript isoforms that differ in exon and TSS usage, we determined the exact structure in MDA-PCa-2b and LNCaP cells by RACE. A common TSS for *ARLNC1* was found in both cell lines, and the ~2.8-kb transcript isoform was further confirmed by northern blot analysis (Supplementary Fig. 3c). Single-molecule FISH (smFISH) revealed that approximately 100 molecules of ARLNC1 transcript existed per MDA-PCa-2b cell (Supplementary Fig. 3d,e). Using smFISH and qPCR, we also found that ARLNC1 molecules were distributed equally between the nuclear and cytoplasmic cellular compartments (Supplementary Fig. 3f,g).

***ARLNC1* transcription is directly regulated by AR.** Because ARLNC1 was identified as an AR-regulated lncRNA, we inspected the promoter region of the *ARLNC1* gene for AR occupancy and identified an androgen-induced AR peak in AR ChIP-seq data from both DHT-stimulated VCaP and LNCaP cells (Fig. 3a). Notably, this AR-binding site was also observed in prostate tissue samples and contained a canonical androgen response element[33] (Fig. 3a). These observations were corroborated by ChIP–qPCR in MDA-PCa-2b cells, which showed the highest level of ARLNC1 expression (Fig. 3b). Considering the observation that ARLNC1 expression is prostate tissue specific, while AR expression is not as much, we searched for additional regulators (transcription factors and epigenetic modifiers) of the *ARLNC1* gene (Supplementary Fig. 4a). Motif analysis of the *ARLNC1* promoter region identified several transcription factor binding sites, including a FOXA1 response element. To further validate *ARLNC1* gene regulation by AR and FOXA1, we evaluated ARLNC1 transcript levels following AR or FOXA1 knockdown. AR or FOXA1 loss resulted in decreased expression of ARLNC1, along with other canonical AR target genes that served as positive controls (Fig. 3c and Supplementary Fig. 4b). ChIP–seq and ChIP–qPCR analyses additionally confirmed the putative FOXA1-binding motif on the *ARLNC1* promoter (Supplementary Fig. 4c). Together, these observations suggest that ARLNC1 is directly regulated by AR and modestly regulated by FOXA1, which partially explains the tissue-specific expression pattern of ARLNC1, as expression of these two transcription factors overlaps nearly exclusively in prostate tissue[37,38] (Supplementary Fig. 4d).

ARLNC1 regulates AR signaling. To elucidate the function of ARLNC1 in prostate cancer, we performed gene expression profiling of wild-type and ARLNC1-knockdown MDA-PCa-2b cells (Fig. 4a). Gene ontology (GO) pathway enrichment analysis of the differentially expressed genes revealed deregulation of four main biological activities: apoptosis, cell proliferation, DNA damage response and androgen signaling (Fig. 4a). The significant decrease in AR target gene expression is particularly interesting given the fact that ARLNC1 is regulated by AR, suggesting a positive feedback loop between ARLNC1 and AR signaling. To confirm this observation, we generated an AR target gene signature from MDA-PCa-2b cells stimulated with DHT (Supplementary Fig. 5a and Supplementary Table 2) and performed gene set enrichment analysis (GSEA) using this gene signature (Fig. 4b). Knockdown

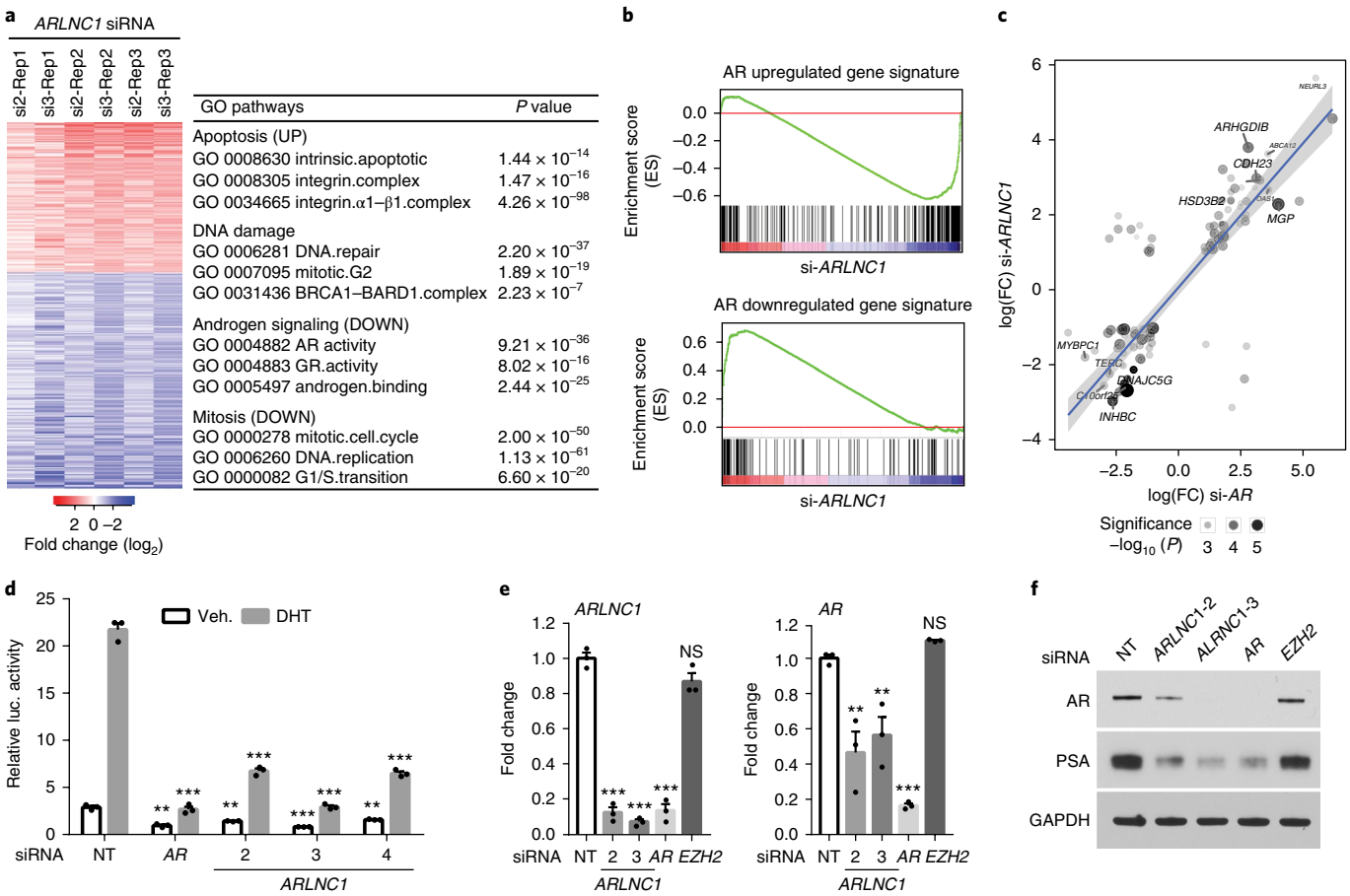

Fig. 4 | ARLNC1 loss attenuates AR signaling. a, Gene expression profiling for ARLNC1 knockdown in MDA-PCa-2b cells ($n = 3$ biologically independent cell cultures for each siRNA). The chart presents the top enriched pathways following ARLNC1 knockdown, identified using GO enrichment analysis (RandomSet test). **b**, GSEA showing significant enrichment of the ARLNC1-regulated gene set with respect to the AR target gene sets ($n = 3$ independent gene expression profiles). Shown are enrichment plots for gene sets consisting of genes positively regulated by AR (top) and genes negatively regulated by AR (bottom). **c**, Comparison of ARLNC1-regulated and AR target genes based on RNA-seq following knockdown of AR and ARLNC1. Significant genes and their log-transformed fold changes in either of the conditions are shown ($n = 2$ independent cell cultures per-condition). Combined significance levels, determined by a limma-moderated *t* test (across both knockdowns), are indicated by circle size. **d**, siRNA knockdown of *ARLNC1* in MDA-PCa-2b cells impairs AR signaling as determined by AR reporter gene assay. siRNA against *AR* serves as a positive control for inhibition of AR signaling. Mean ± s.e.m. values are shown, $n = 3$ biologically independent cell cultures. $^{**}P < 0.01$, $^{***}P = 0.0001$, determined by ANOVA with Dunnett correction. **e**, qRT-PCR analysis of *ARLNC1* and *AR* in MDA-PCa-2b cells transfected with siRNAs against *ARLNC1*, *AR*, *EZH2* or non-specific control (NT). siRNA against *AR* serves as a positive control for inhibition of AR signaling, while siRNA against *EZH2* serves as a negative control. Mean ± s.e.m. values are shown, $n = 3$. $^{**}P < 0.01$, $^{***}P = 0.0001$, determined by ANOVA with Dunnett correction. **f**, Immunoblots of AR, PSA and GAPDH in MDA-PCa-2b cells transfected with siRNAs against *ARLNC1*, *AR*, *EZH2* or non-specific control (NT). The experiments were repeated three times independently with similar results. Uncropped images are shown in Supplementary Fig. 9.

of ARLNC1 led to suppression of genes positively regulated by AR and upregulation of genes negatively regulated by AR (Fig. 4b,c and Supplementary Fig. 5b). This was further confirmed by an AR reporter activity assay (Fig. 4d and Supplementary Fig. 5c), as well as qPCR analysis of AR target genes (Supplementary Fig. 5d). Interestingly, ARLNC1 knockdown also had a significant effect on the mRNA and protein levels of AR (Fig. 4e,f), suggesting direct regulation of AR by ARLNC1. However, we found that ARLNC1 overexpression did not affect AR and its signaling cascade (Supplementary Fig. 5e).

In situ colocalization of ARLNC1 and *AR* transcripts. Noncoding RNAs have been shown to target mRNAs via direct or indirect RNA–RNA interaction[9,40–42]. To identify target mRNAs that could interact with ARLNC1, we performed unbiased prediction of RNA–RNA interactions using IntraRNA[43,44]. Interestingly, the 3′ UTR of the *AR* transcript was identified as a target of ARLNC1 (Fig. 5a and Supplementary Fig. 6a). An in vitro RNA–RNA interaction assay between the 3′ UTR of *AR* and full-length ARLNC1 confirmed this in silico prediction (Fig. 5b). To evaluate this interaction in the context of the cellular environment, multiplexed smFISH for *AR* and ARLNC1 transcripts was performed in MDA-PCa-2b cells. On co-staining of MDA-PCa-2b cells for either a combination of *AR* transcripts and a panel of lncRNAs or ARLNC1 and a panel of mRNAs, we observed specific colocalization of *AR* and ARLNC1 transcripts in the nucleus within foci that were typically larger than individual molecules (Fig. 5c–e). The extent of colocalization was much higher than that expected from coincidental colocalization with an abundant transcript, such as MALAT1 or *GAPDH* (Fig. 5c–e). More specifically, colocalization typically occurred at a stoichiometry of 2:1 ARLNC1/*AR*, which accounted for ~10–20% of all *AR* and ARLNC1 transcripts in the cell (Supplementary Fig. 6b). Furthermore, *AR*–ARLNC1 colocalization was observed in *ARLNC1*-positive prostate cancer tissues (Fig. 5f,g).

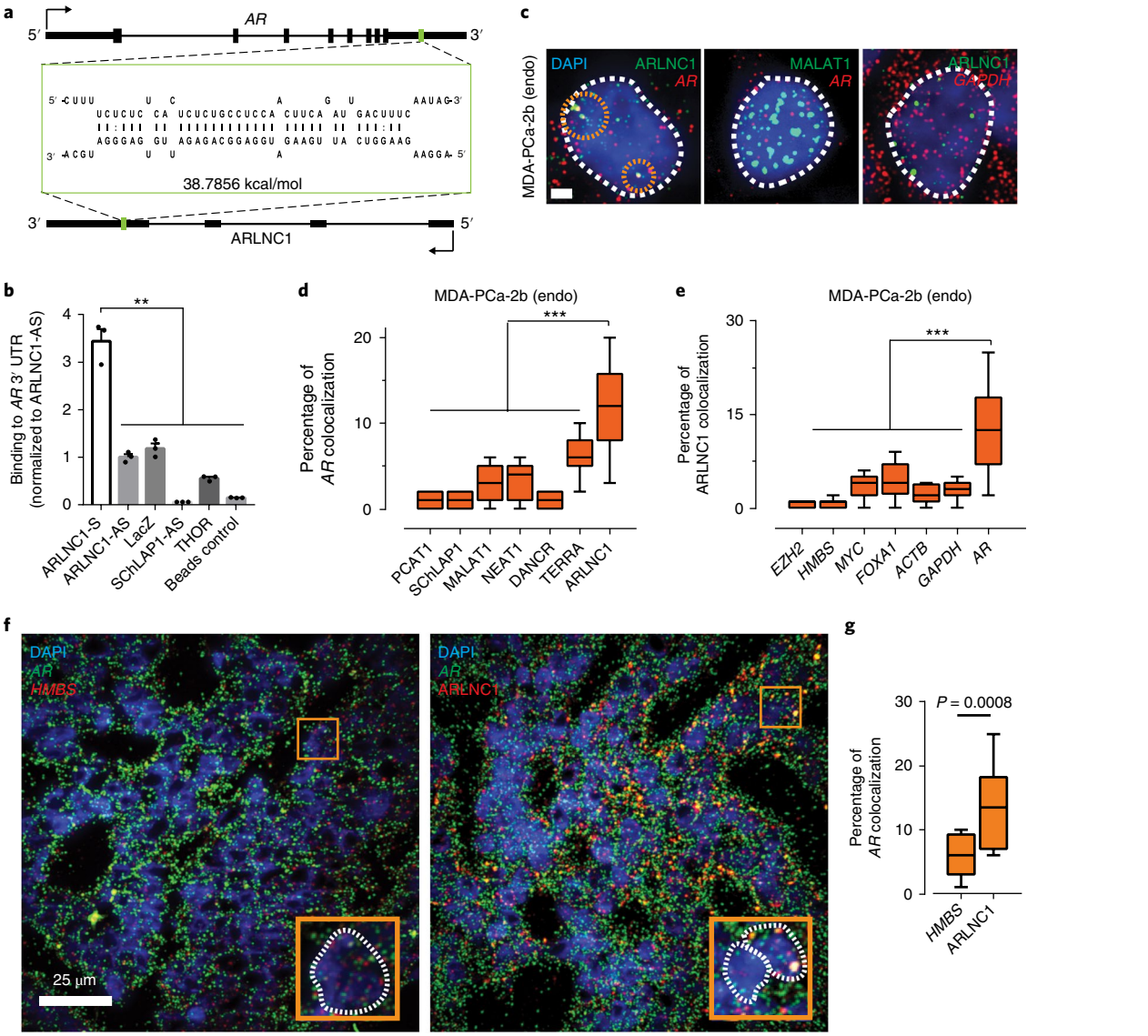

Fig. 5 | In situ colocalization of *AR* mRNA and ARLNC1 in prostate cancer cells. a, Schematic of the predicted RNA–RNA interaction between ARLNC1 and the 3′ UTR of *AR*. **b**, ARLNC1 interacts with the *AR* 3′ UTR in an in vitro RNA–RNA interaction assay. Compared to a panel of control RNAs (ARLNC1 antisense, LacZ, SChLAP1-AS, THOR), ARLNC1 binds to *AR* 3′ UTR-1–980 with high affinity. The binding affinity was quantified by qPCR analysis of the *AR* 3′ UTR. Data were normalized to the ARLNC1-AS control. Mean ± s.e.m. are shown, $n = 3$. $^{**}P < 0.001$, by two-tailed Student's *t* test. **c**–**e**, smFISH depiction of *AR*–ARLNC1 colocalization in situ. **c**, Representative pseudocolored images of MDA-PCa-2b cell nuclei stained for the appropriate endogenous (endo) transcripts (green, red) and with DAPI (nucleus, blue). Scale bar, 5 μm. The orange circles represent regions of colocalization. **d**,**e**, Quantification of the percentage of *AR* or ARLNC1 molecules colocalizing with a panel of lncRNAs (**d**) or mRNAs (**e**). The center line and whiskers depict the median and range, respectively, and the box extends from the 25th to the 75th percentile ($n = 50$ cells for each sample aggregated from 3 independent experiments). $^{***}P < 0.0001$, by two-tailed Student's *t* test. **f**, Representative pseudocolored images of ARLNC1-positive prostate cancer tissues stained with DAPI (nucleus, blue) and for *AR* (green), *HMBS* (red) or ARLNC1 (red) transcripts (smFISH). Inset, 5.5 × 5.5 μm² zoomed-in view of the box within the main panel. **g**, Quantification of the percentage of *AR* molecules colocalizing with *HMBS* transcripts or ARLNC1. The center line and whiskers depict the median and range, respectively, and the box extends from the 25th to the 75th percentile ($n = 15$ field-of-views for each sample aggregated from 3 independent tissues). $P < 0.001$, by two-tailed Student's *t* test.

Using an in vitro RNA–RNA binding assay, we identified nucleotides 700–1300 of ARLNC1 to be critical for binding to the *AR* 3′ UTR (Fig. 6a,b). To confirm this observation within the cellular context, we ectopically overexpressed different fragments of ARLNC1 together with *AR* in U2OS osteosarcoma cells. In this exogenous system, colocalization of *AR* and ARLNC1 was once again demonstrated, wherein colocalization was dependent on the presence of nucleotides 700–1300 of ARLNC1 (Fig. 6c,d and Supplementary Fig. 6c). Furthermore, incubation with antisense oligonucleotides (ASOs) that blocked the interaction site led to a significant reduction in ARLNC1–*AR* interaction in vitro and in situ (Fig. 6e,f and Supplementary Fig. 6d,e). Decreased AR signaling was also observed following blocking of this interaction (Fig. 6g and Supplementary Fig. 6f).

ARLNC1 regulates the cytoplasmic levels of *AR* transcripts. We then sought to delineate the mechanism of ARLNC1-mediated AR regulation. We first monitored the stability of these two transcripts and found that *AR* and ARLNC1 have similar half-lives of ~9 h (Supplementary Fig. 6g). As ARLNC1 depletion resulted in a

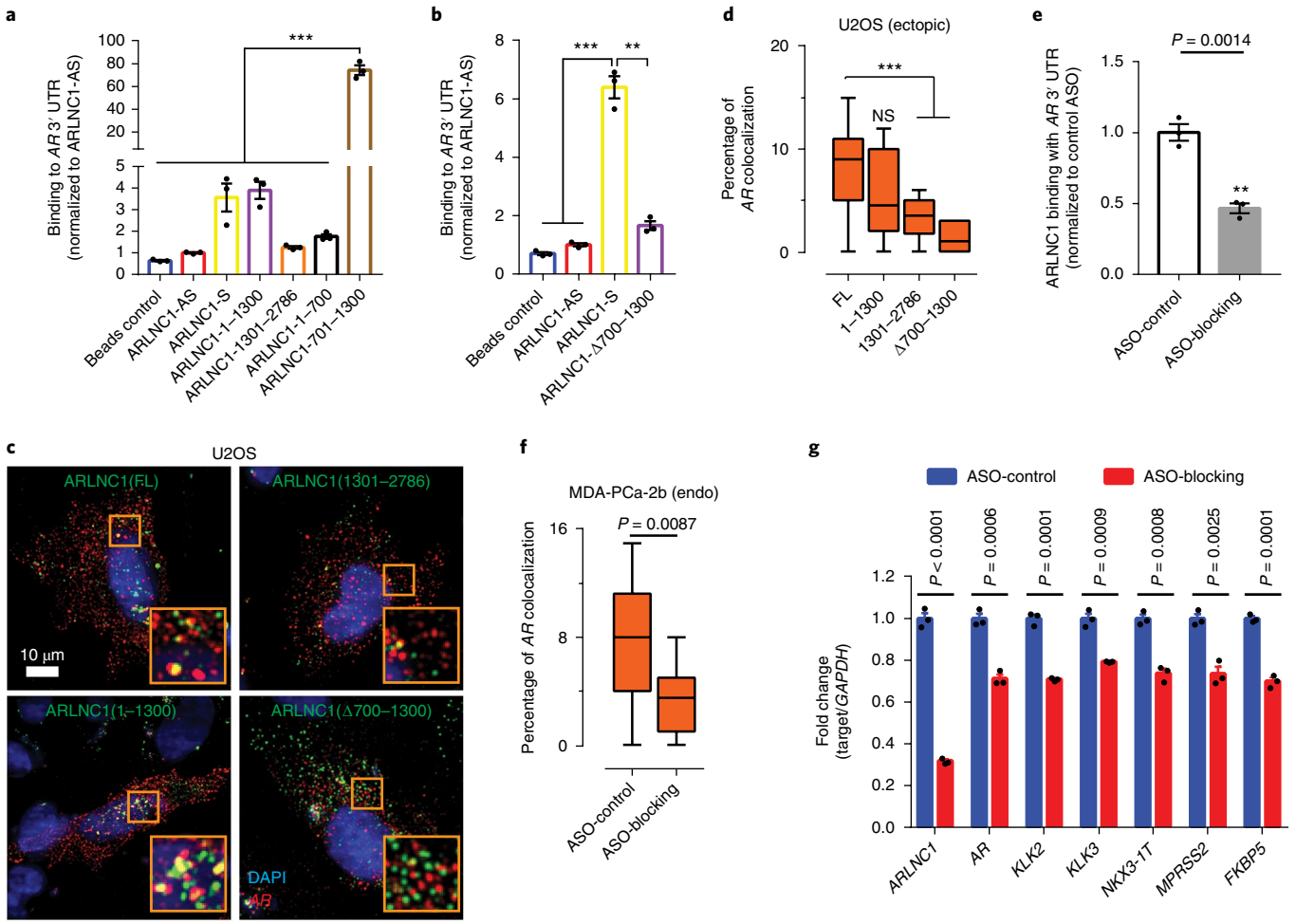

Fig. 6 | Identification of the ARLNC1 fragment mediating RNA–RNA interaction with *AR* mRNA. a, In vitro RNA–RNA interaction assay identifies nucleotides 700–1300 on ARLNC1 as critical binding site to *AR* 3′ UTR-1–980. ARLNC1 fragments covering nucleotides 700–1300 display comparable or higher *AR* 3′ UTR binding affinity than ARLNC1-S, with ARLNC1-700–1300 exhibiting the highest binding affinity. Data were normalized to the ARLNC1-AS control. Mean ± s.e.m. values are shown, $n = 3$. ***P (adjusted) = 0.0001, determined by ANOVA with Dunnett's multiple-comparisons test. **b**, Deletion of nucleotides 700–1300 on ARLNC1 results in impaired binding to the *AR* 3′ UTR, as shown by in vitro RNA–RNA interaction assay. Data were normalized to the ARLNC1-AS control. Mean ± s.e.m. values are shown, $n = 3$. ***$P = 0.0001$, **$P = 0.0003$, by two-tailed Student's t test. **c**,**d**, smFISH shows that nucleotides 700–1300 in ARLNC1 are important for colocalization in situ. **c**, Representative pseudocolored images of U2OS cells stained with DAPI (nucleus, blue) and for ARLNC1 (green) and *AR* transcripts (red). Inset, 10 × 10 μm² zoomed-in view of the orange box in the main image. **d**, Quantification of the percentage of *AR* molecules colocalizing with various ARLNC1 fragments. The center line and whiskers depict the median and range, respectively, and the box extends from the 25th to the 75th percentile ($n = 50$ cells for each sample aggregated from 3 independent experiments). ***$P < 0.0001$, by two-tailed Student's t test. NS, not significant. **e**, ASOs targeting nucleotides 700–1300 on the ARLNC1 transcript (ASO-blocking pool) inhibit ARLNC1 interaction with the *AR* 3′ UTR. In vitro RNA–RNA interaction assays were performed using ARLNC1 and the *AR* 3′ UTR, with the addition of the blocking ASO pool or control ASO. Data were normalized to the control ASO. Mean ± s.e.m. values are shown, $n = 3$. $P = 0.0014$, by two-tailed Student's t test. **f**, smFISH shows that ASOs targeting nucleotides 700–1300 on the ARLNC1 transcript (ASO-blocking) inhibit ARLNC1 colocalization with *AR* in situ. Quantification is shown of the percentage of *AR* transcripts colocalizing with ARLNC1 after various treatments in MDA-PCa-2b cells. The center line and whiskers depict the median and range, respectively, and the box extends from the 25th to the 75th percentile ($n = 50$ cells for each sample aggregated from 3 independent experiments). The P value was computed by two-tailed Student's t test. **g**, qPCR analysis of *ARLNC1*, *AR* and AR signaling genes (*KLK2*, *KLK3*, *NKX3-1*, *TMPRSS2* and *FKBP5*) in MDA-PCa-2b cells transfected with control or blocking ASOs targeting the interaction site between ARLNC1 and the *AR* 3′ UTR. Mean ± s.e.m. values are shown, $n = 3$. Significance was determined by two-tailed Student's t test.

striking reduction of AR protein levels, much more than could be explained by *AR* transcript reduction, we hypothesized that ARLNC1 could affect *AR* post-transcriptionally. To test this hypothesis, we tracked the subcellular localization of *AR* transcripts using smFISH after depleting ARLNC1. We confirmed successful in situ knockdown of ARLNC1 using siRNAs, antisense oligonucleotide (ASO) and the blocking oligonucleotides that targeted the ARLNC1–*AR* interaction (ASO-blocking) in MDA-PCa-2b cells (Supplementary Fig. 6h,i). Quantification of the subcellular distribution of ARLNC1 suggested that the nuclear fraction of ARLNC1 was enriched only in the *ARLNC1* siRNA (si-*ARLNC1*) condition (Supplementary Fig. 6j), a result expected for siRNAs that are typically more functional in the cytosol[45]. Surprisingly, ARLNC1 knockdown or obstruction of the *AR*–ARLNC1 interaction increased the nuclear *AR* fraction by dramatically decreasing cytoplasmic levels of the *AR* transcript (Fig. 7a,b and Supplementary Fig. 6k–l). This observation was further supported by BrU-seq and BrUChase-seq, two high-throughput tools that monitor transcript synthesis and stability. On ARLNC1

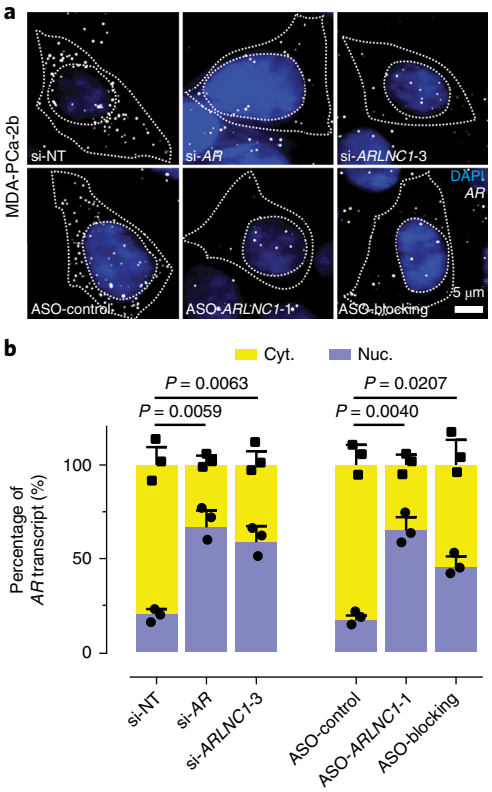

Fig. 7 | ARLNC1 regulates the cytoplasmic level of the *AR* transcript. **a**, ARLNC1 regulates *AR* post-transcriptionally by specifically affecting cytoplasmic *AR* mRNA. Representative pseudocolored images are shown of MDA-PCa-2b cells stained for DAPI (nucleus, blue) and *AR* (gray) after treatment with siRNA against *AR* (si-*AR*), siRNA against *ARLNC1* (si-*ARLNC1*-3), ASO against *ARLNC1* (ASO-*ARLNC1*-1) or blocking ASO against the *AR*–ARLNC1 colocalizing segment (ASO-blocking). Quantification of knockdown is shown in Supplementary Fig. 6k,l. **b**, Fractional column plots depicting the nucleo-cytoplasmic distribution of *AR* mRNA after the various treatment conditions in **a**, as computed using smFISH. Mean ± s.e.m. values are shown, $n = 3$ independent experiments and 60 cells analyzed for each sample. The *P* values were computed by comparing to si-NT- or ASO-control-treated cells, by two-tailed Student's *t* test.

knockdown, the synthesis rate of the *AR* transcript remained the same (Supplementary Fig. 6m), while the stability of the transcript decreased, particularly through the 3′ UTR (Supplementary Fig. 6n). Taken together, our data suggest that ARLNC1 regulates the cytoplasmic levels of *AR* transcripts. Furthermore, the transcriptional coupling between *AR* and ARLNC1 transcripts is mediated by direct interactions that are encoded in their sequences.

Inhibition of ARLNC1 delays prostate cancer growth in vitro and in vivo. Having established a role for ARLNC1 in the regulation of AR signaling, we further evaluated the biological effects of ARLNC1 in prostate cancer cell lines. GO pathway enrichment analysis of the knockdown microarray data showed that ARLNC1-regulated genes were involved in cell proliferation and apoptosis (Fig. 4a). Knockdown of ARLNC1 had a significant effect on the proliferation of AR-dependent MDA-PCa-2b and LNCaP cells, but had no effect on AR-negative DU145 and PC3 cells (Fig. 8a and Supplementary Fig. 7a,b). Knockdown of ARLNC1 also resulted in increased apoptosis in AR-positive prostate cancer cells (Fig. 8b and Supplementary Fig. 7c). Notably, these results translated to effects in vivo, as cells expressing shRNA targeting *ARLNC1* formed smaller tumors in mice when compared to cells expressing non-targeting shRNA (Fig. 8c), thus suggesting that ARLNC1 is an important survival factor for AR-dependent prostate cancer.

Because modulation of ARLNC1 expression levels resulted in a striking proliferation phenotype, we hypothesized that ARLNC1 inhibition could be used therapeutically for the treatment of prostate cancer. ASOs have recently been shown to be effective in targeting RNA in vivo[46–49]; thus, we designed ASOs targeting the ARLNC1 transcript (Supplementary Fig. 7d). Transfection of ASOs resulted in strong knockdown efficiency (Supplementary Fig. 7e), and ASO-mediated knockdown resulted in similar effects on gene expression profiling to siRNA (Fig. 8d,e and Supplementary Fig. 7f). Furthermore, AR-positive cells transfected with *ARLNC1* ASOs exhibited retarded growth, similar to those treated with siRNAs (Fig. 8f). To evaluate the therapeutic potential of *ARLNC1* ASOs in vivo, we first assessed the cellular free-uptake efficiency of *ARLNC1* ASOs, a prerequisite for ASO therapeutic use. Notably, several ASOs significantly reduced ARLNC1 levels through free uptake (Supplementary Fig. 7g). Free uptake of *ARLNC1* ASOs led to a significant decrease in the proliferation capacity of MDA-PCa-2b cells in both normal cell culture and 3D sphere conditions (Supplementary Fig. 7h–j). Treatment of mice bearing MDA-PCa-2b xenografts with *ARLNC1*-targeting ASOs led to significant decreases in tumor growth compared to control ASO (Fig. 8g,h and Supplementary Fig. 8a–e). Taken together, these data, along with the association of ARLNC1 with aggressive androgen signaling (Supplementary Fig. 8f–j), suggest that ARLNC1 plays a critical role in the proliferation of AR-dependent prostate cancer and can be effectively exploited as a therapeutic target.

Discussion

As AR signaling remains a significant driver of CRPC pathogenesis, it is imperative to generate novel strategies to target this pathway. Even with the addition of enzalutamide or abiraterone to CRPC treatment regimens, progression invariably occurs. Exploiting players other than AR itself that are pivotal to maintaining the magnitude of the androgen response is an alternative approach. Our comprehensive profiling of AR-regulated, prostate cancer–associated lncRNAs identified the top-ranking candidate ARLNC1 that we functionally characterized. We identified a positive feedback loop between ARLNC1 and AR that maintains the androgen transcriptional program in AR-positive prostate cancer cells, specifically through regulating the cellular levels of AR (Fig. 8i). The mechanism we identified echoes previous studies on lncRNAs—1/2-sbsRNAs[42], BACE1-AS[9] and TINCR[41], which highlights the role of lncRNA in increasing or decreasing RNA stability.

As a novel noncoding regulator of AR signaling, ARLNC1 has the potential to be not only a mechanistic biomarker but also a therapeutic target for advanced prostate cancer. In addition, the fact that it acts upstream of AR signaling presents the possibility that targeting ARLNC1 may afford an additional option to patients that have de novo or acquired resistance to therapies targeting AR itself (that is, enzalutamide or abiraterone). Furthermore, specific antisense nucleotides targeting ARLNC1, which we demonstrate to be specifically expressed in the prostate, could circumvent undesirable side effects that occur in other tissues with exposure to androgen synthesis inhibitors or anti-androgens.

Although we have identified a new node of the AR signaling network that can be therapeutically targeted, the molecular mechanism through which ARLNC1 regulates *AR* transcript levels remains to be fully characterized. At this time, it is unclear whether the physical interaction between the *AR* 3′ UTR and ARLNC1 functions with the aid of additional RNA-binding proteins (for example, HuR) and/or RNAs in vivo[50,51]. Nonetheless, the application of ASOs has ushered in an exciting era that makes it possible to target previously 'undruggable' molecules directly at the transcript level, such as ARLNC1, which is likely to yield promising opportunities in cancer treatment.

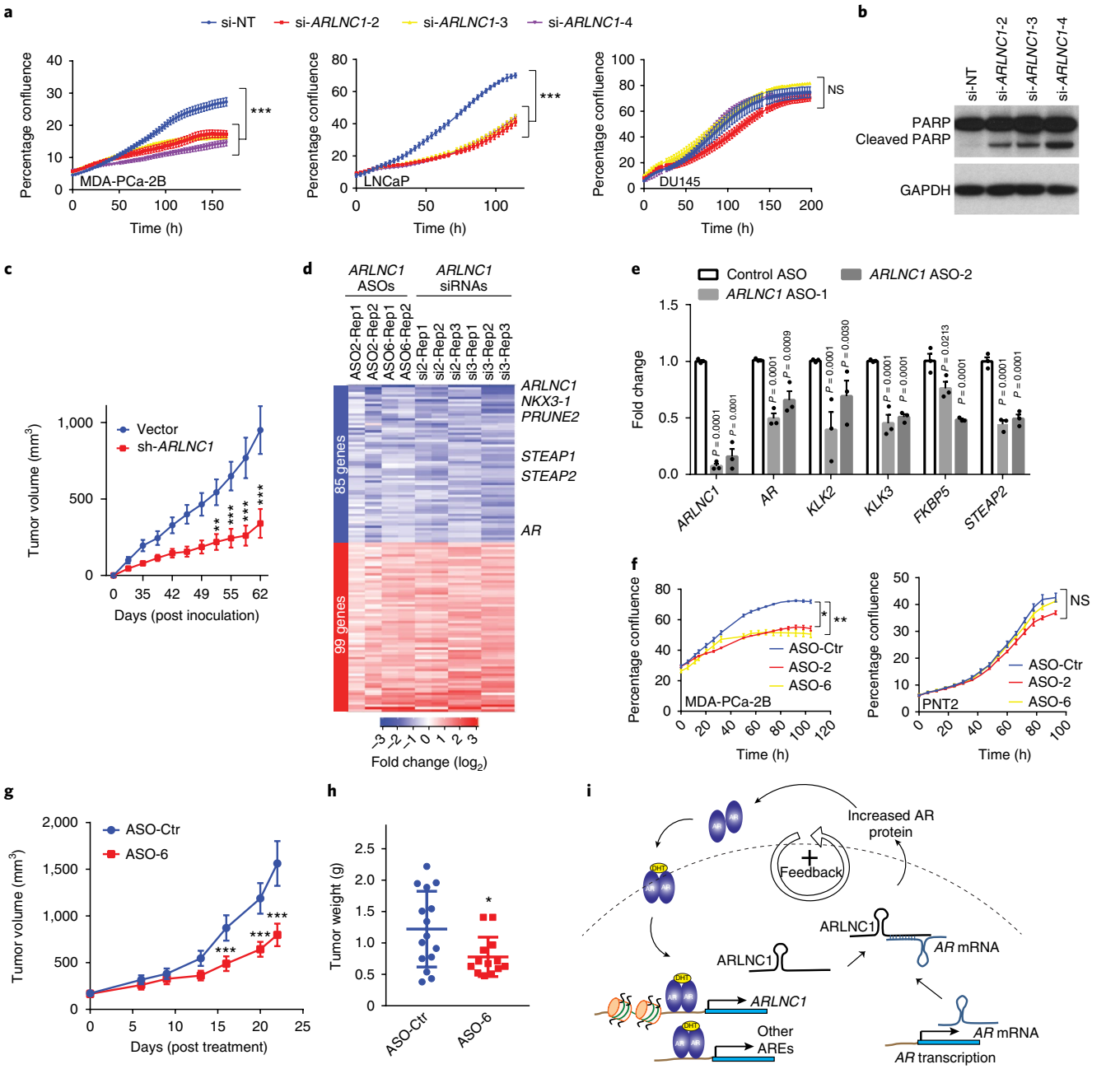

Fig. 8 | ARLNC1 as a therapeutic target in AR-positive prostate cancer models. a, siRNA-mediated knockdown of ARLNC1 in vitro in AR-positive prostate cancer cell lines (MDA-PCa-2b and LNCaP) inhibits cell proliferation. The AR-negative prostate cell line DU145 serves as a negative control. Mean ± s.d. values are shown, $n = 6$ independent cell cultures per group, $^{**}P$ (adjusted) = 0.0001 compared to si-NT-treated cells, by one-way ANOVA with Dunnett's multiple-comparisons test; NS, not significant. **b**, ARLNC1 loss leads to increased apoptosis as shown by western blot analysis of PARP and cleaved PARP in LNCaP cells following ARLNC1 knockdown. The experiment was repeated independently three times with similar results. Uncropped images are shown in Supplementary Fig. 9. **c**, Tumor growth of LNCaP-AR cells expressing shRNA targeting *ARLNC1* or shRNA vector. Mean ± s.e.m. values are shown. $n = 10$ independent tumors, $^{***}P < 0.0001$, $^{**}P = 0.0007$, as determined by two-tailed Student's *t* test. **d**, Gene expression profiling for siRNA-mediated or ASO-mediated ARLNC1 knockdown in MDA-PCa-2b cells. The numbers above the heat map represent the specific microarray replicates. **e**, qRT-PCR analysis of *ARLNC1*, *AR* and AR targets (*KLK2*, *KLK3*, *FKBP5* and *STEAP2*) in MDA-PCa-2b cells transfected with ASOs against *ARLNC1*. Data were normalized to a housekeeping gene, and the levels in control ASO-treated cells were set to 1. Mean ± s.e.m. values are shown, $n = 3$. Adjusted *P* values were determined by one-way ANOVA with Dunnett correction for multiple comparisons. **f**, Transfection of ASOs targeting *ARLNC1* in AR-positive MDA-PCa-2b cells inhibits cell proliferation. The AR-negative prostate cell line PNT2 serves as a negative control. Mean ± s.e.m. values are shown, $n = 6$ independent cell cultures per treatment group. $^{*}P$ (adjusted) = 0.0112, $^{**}P$ (adjusted) = 0.0065, NS: not significant; compared to the control-ASO group by one-way ANOVA with Dunnett correction for multiple comparisons. **g**,**h**, Effect of ASO treatment on the growth of MDA-PCa-2b xenografts in male athymic nude mice, with control ASO ($n = 15$) or *ARLNC1* ASO ($n = 13$) treatment subcutaneously at 50 mg per kg body weight, five times per week for 3 weeks. Tumors were measured by caliper biweekly (**g**) and tumor weights were measured at the end point (**h**). Mean ± s.d. values are shown. $^{*}P = 0.0251$, $^{***}P < 0.0001$; compared to control ASO by two-tailed Student's *t* test. **i**, A model depicting the positive feedback loop between ARLNC1 and AR that is critical for prostate cancer growth.

Methods

Methods, including statements of data availability and any associated accession codes and references, are available at https://doi.org/10.1038/s41588-018-0120-1.

Received: 7 February 2017; Accepted: 23 March 2018;
Published online: 28 May 2018

References

1. Mercer, T. R., Dinger, M. E. & Mattick, J. S. Long non-coding RNAs: insights into functions. *Nat. Rev. Genet.* **10**, 155–159 (2009).
2. Wang, K. C. & Chang, H. Y. Molecular mechanisms of long noncoding RNAs. *Mol. Cell* **43**, 904–914 (2011).
3. Rinn, J. L. & Chang, H. Y. Genome regulation by long noncoding RNAs. *Annu. Rev. Biochem.* **81**, 145–166 (2012).
4. Rinn, J. L. et al. Functional demarcation of active and silent chromatin domains in human HOX loci by noncoding RNAs. *Cell* **129**, 1311–1323 (2007).
5. Lee, N., Moss, W. N., Yario, T. A. & Steitz, J. A. EBV noncoding RNA binds nascent RNA to drive host PAX5 to viral DNA. *Cell* **160**, 607–618 (2015).
6. Wutz, A., Rasmussen, T. P. & Jaenisch, R. Chromosomal silencing and localization are mediated by different domains of Xist RNA. *Nat. Genet.* **30**, 167–174 (2002).
7. Prensner, J. R. et al. The long noncoding RNA SChLAP1 promotes aggressive prostate cancer and antagonizes the SWI/SNF complex. *Nat. Genet.* **45**, 1392–1398 (2013).
8. Gupta, R. A. et al. Long non-coding RNA HOTAIR reprograms chromatin state to promote cancer metastasis. *Nature* **464**, 1071–1076 (2010).
9. Faghihi, M. A. et al. Expression of a noncoding RNA is elevated in Alzheimeras disease and drives rapid feed-forward regulation of β-secretase. *Nat. Med* **14**, 723–730 (2008).
10. Iyer, M. K. et al. The landscape of long noncoding RNAs in the human transcriptome. *Nat. Genet.* **47**, 199–208 (2015).
11. Malik, R. et al. The lncRNA PCAT29 inhibits oncogenic phenotypes in prostate cancer. *Mol. Cancer Res.* **12**, 1081–1087 (2014).
12. Shukla, S. et al. Identification and validation of PCAT14 as prognostic biomarker in prostate cancer. *Neoplasia* **18**, 489–499 (2016).
13. Lu-Yao, G. L. et al. Fifteen-year survival outcomes following primary androgen-deprivation therapy for localized prostate cancer. *JAMA Intern. Med.* **174**, 1460–1467 (2014).
14. Huggins, C. & Hodges, C. V. Studies on prostatic cancer. I. The effect of castration, of estrogen and of androgen injection on serum phosphatases in metastatic carcinoma of the prostate. 1941. *J. Urol.* **167**, 948–951 (2002).
15. The Veterans Administration Co-operative Urological Research Group. Treatment and survival of patients with cancer of the prostate. *Surg. Gynecol. Obstet.* **124**, 1011–1017 (1967).
16. Chen, Y., Sawyers, C. L. & Scher, H. I. Targeting the androgen receptor pathway in prostate cancer. *Curr. Opin. Pharmacol.* **8**, 440–448 (2008).
17. Wong, Y. N., Ferraldeschi, R., Attard, G. & de Bono, J. Evolution of androgen receptor targeted therapy for advanced prostate cancer. *Nat. Rev. Clin. Oncol.* **11**, 365–376 (2014).
18. Mukherji, D., Pezaro, C. J. & De-Bono, J. S. MDV3100 for the treatment of prostate cancer. *Expert Opin. Investig. Drugs* **21**, 227–233 (2012).
19. Scher, H. I. et al. Increased survival with enzalutamide in prostate cancer after chemotherapy. *N. Engl. J. Med.* **367**, 1187–1197 (2012).
20. Tran, C. et al. Development of a second-generation antiandrogen for treatment of advanced prostate cancer. *Science* **324**, 787–790 (2009).
21. Scher, H. I. et al. Antitumour activity of MDV3100 in castration-resistant prostate cancer: a phase 1-2 study. *Lancet* **375**, 1437–1446 (2010).
22. Stein, M. N., Goodin, S. & Dipaola, R. S. Abiraterone in prostate cancer: a new angle to an old problem. *Clin. Cancer Res.* **18**, 1848–1854 (2012).
23. Reid, A. H. et al. Significant and sustained antitumor activity in post-docetaxel, castration-resistant prostate cancer with the CYP17 inhibitor abiraterone acetate. *J. Clin. Oncol.* **28**, 1489–1495 (2010).
24. de Bono, J. S. et al. Abiraterone and increased survival in metastatic prostate cancer. *N. Engl. J. Med.* **364**, 1995–2005 (2011).
25. Watson, P. A., Arora, V. K. & Sawyers, C. L. Emerging mechanisms of resistance to androgen receptor inhibitors in prostate cancer. *Nat. Rev. Cancer* **15**, 701–711 (2015).
26. Antonarakis, E. S. et al. AR-V7 and resistance to enzalutamide and abiraterone in prostate cancer. *N. Engl. J. Med.* **371**, 1028–1038 (2014).
27. Attard, G., Richards, J. & de Bono, J. S. New strategies in metastatic prostate cancer: targeting the androgen receptor signaling pathway. *Clin. Cancer Res.* **17**, 1649–1657 (2011).
28. Hearn, J. W. et al. HSD3B1 and resistance to androgen-deprivation therapy in prostate cancer: a retrospective, multicohort study. *Lancet Oncol.* **17**, 1435–1444 (2016).
29. Chan, S. C., Li, Y. & Dehm, S. M. Androgen receptor splice variants activate androgen receptor target genes and support aberrant prostate cancer cell growth independent of canonical androgen receptor nuclear localization signal. *J. Biol. Chem.* **287**, 19736–19749 (2012).
30. Robinson, D. et al. Integrative clinical genomics of advanced prostate cancer. *Cell* **161**, 1215–1228 (2015).
31. Visakorpi, T. et al. In vivo amplification of the androgen receptor gene and progression of human prostate cancer. *Nat. Genet.* **9**, 401–406 (1995).
32. Asangani, I. A. et al. Therapeutic targeting of BET bromodomain proteins in castration-resistant prostate cancer. *Nature* **510**, 278–282 (2014).
33. Roche, P. J., Hoare, S. A. & Parker, M. G. A consensus DNA-binding site for the androgen receptor. *Mol. Endocrinol.* **6**, 2229–2235 (1992).
34. Pomerantz, M. M. et al. The androgen receptor cistrome is extensively reprogrammed in human prostate tumorigenesis. *Nat. Genet.* **47**, 1346–1351 (2015).
35. Cancer Genome Atlas Research Network. The molecular taxonomy of primary prostate cancer. *Cell* **163**, 1011–1025 (2015).
36. Takayama, K. et al. Androgen-responsive long noncoding RNA CTBP1-AS promotes prostate cancer. *EMBO J.* **32**, 1665–1680 (2013).
37. GTEx Consortium. The Genotype-Tissue Expression (GTEx) pilot analysis: multitissue gene regulation in humans. *Science* **348**, 648–660 (2015).
38. Mele, M. et al. The human transcriptome across tissues and individuals. *Science* **348**, 660–665 (2015).
39. Rhodes, D. R. et al. Oncomine 3.0: genes, pathways, and networks in a collection of 18,000 cancer gene expression profiles. *Neoplasia* **9**, 166–180 (2007).
40. Engreitz, J. M. et al. RNA-RNA interactions enable specific targeting of noncoding RNAs to nascent pre-mRNAs and chromatin sites. *Cell* **159**, 188–199 (2014).
41. Kretz, M. et al. Control of somatic tissue differentiation by the long non-coding RNA TINCR. *Nature* **493**, 231–235 (2013).
42. Gong, C. & Maquat, L. E. lncRNAs transactivate STAU1-mediated mRNA decay by duplexing with 3′ UTRs via Alu elements. *Nature* **470**, 284–288 (2011).
43. Gawronski, A. R. et al. MechRNA: prediction of lncRNA mechanisms from RNA-RNA and RNA-protein interactions. *Bioinformatics* (2018) https://doi.org/10.1093/bioinformatics/bty208
44. Mann, M., Wright, P. R. & Backofen, R. IntaRNA 2.0: enhanced and customizable prediction of RNA–RNA interactions. *Nucleic Acids Res.* **45**, W435–W439 (2017).
45. Lennox, K. A. & Behlke, M. A. Cellular localization of long non-coding RNAs affects silencing by RNAi more than by antisense oligonucleotides. *Nucleic Acids Res.* **44**, 863–877 (2016).
46. Meng, L. et al. Towards a therapy for Angelman syndrome by targeting a long non-coding RNA. *Nature* **518**, 409–412 (2015).
47. Wheeler, T. M. et al. Targeting nuclear RNA for in vivo correction of myotonic dystrophy. *Nature* **488**, 111–115 (2012).
48. Hua, Y. et al. Antisense correction of SMN2 splicing in the CNS rescues necrosis in a type III SMA mouse model. *Genes Dev.* **24**, 1634–1644 (2010).
49. Evers, M. M., Toonen, L. J. & van Roon-Mom, W. M. Antisense oligonucleotides in therapy for neurodegenerative disorders. *Adv. Drug Deliv. Rev.* **87**, 90–103 (2015).
50. Yeap, B. B. et al. Novel binding of HuR and poly(C)-binding protein to a conserved UC-rich motif within the 3'-untranslated region of the androgen receptor messenger RNA. *J. Biol. Chem.* **277**, 27183–27192 (2002).
51. Lebedeva, S. et al. Transcriptome-wide analysis of regulatory interactions of the RNA-binding protein HuR. *Mol. Cell* **43**, 340–352 (2011).

Acknowledgements

We thank A. Poliakov, A. Parolia, V. Kothari and J. Siddiqui for helpful discussions, the University of Michigan Sequencing Core for Sanger sequencing, H. Johansson (LGC-Biosearch) for initial assistance with smFISH probe design, and S. Ellison, S. Gao and K. Giles for critically reading the manuscript and submitting documents. This work was supported in part by NCI Prostate SPORE (P50CA186786 to A.M.C.) and EDRN (U01 CA214170 to A.M.C.) grants. A.M.C. is also supported by the Prostate Cancer Foundation and by the Howard Hughes Medical Institute. A.M.C. is an American Cancer Society Research Professor and a Taubman Scholar of the University of Michigan. R. Malik was supported by a Department of Defense Postdoctoral Award (W81XWH-13-1-0284). Y.Z. is supported by a Department of Defense Early Investigator Research Award (W81XWH-17-1-0134). R. Malik, M.C., Y.S.N., J.C.-Y.T. and Y.Q. were supported by the Prostate Cancer Foundation Young Investigator Award. R. Mehra was supported by a Department of Defense Idea Development Award (W81XWH-16-1-0314). Y.S.N. is supported by a University of Michigan Cellular and Molecular Biology National Research Service Award Institutional Predoctoral Training Grant. S.P. was supported by an AACR-Bayer Prostate Cancer Research Fellowship (16-40-44-PITC). L.X. is supported by a US Department of Defense Postdoctoral Fellowship (W81XWH-16-1-0195). M.B. was supported by NIH DP5 grant OD012160. G.C.S. was supported by the Department of Defense awards W81XWH-14-1-0508 and

W81XWH-14-1-0509. M.U. was funded by the German Research Foundation (DFG grant BA2168/11-1 SPP 1738).

Author contributions

R. Malik, Y.Z., M.C., S.P. and A.M.C. conceived the study and designed the research. Y.Z. and R. Malik performed most of the cellular and molecular biology experiments with the assistance of Y.H., S.Y., S.S., S.K.S., L.X., X.J., S.M.D., X.C., J.T.W. and F.Y.F. M.C. performed most of the bioinformatics analyses with the help of Y.S.N. and M.K.I. S.P., U.P. and M.B. performed all smFISH work, and S.P. performed the mechanistic work-up. J.C.-Y.T. and K.M.J. carried out the in vivo mouse xenograft studies, and Y.Q. performed the 3D sphere model work. L.P.K. performed the histopathological analyses. L.W. and R. Mehra carried out RNA ISH on tissue microarrays, and T.-Y.L. and H.J. performed the statistical analysis for this technique. M.U., A.R.G., R.B. and C.S.S. performed the in silico binding predictions. S.M.F., A.T.W. and S.G. provided ASOs. G.C.S. provided the AR expression construct. M.T.P. and M.L. performed BrU and BrUChase sample preparation. Y.Z., M.C., R. Malik, S.P. and A.M.C. wrote the manuscript. All authors discussed the results and commented on the manuscript.

Competing interests

The University of Michigan has filed a patent on lncRNAs as biomarkers of cancer, and A.M.C., R. Malik, Y.Z., M.C. and S.P. are named as co-inventors. A.M.C. is a co-founder of LynxDx, which is developing lncRNA biomarkers. S.M.F., A.T.W. and S.G. are employees of Ionis Pharmaceuticals, which developed the ASOs against *ARLNC1* that were used in this study.

Additional information

Supplementary information is available for this paper at https://doi.org/10.1038/s41588-018-0120-1.

Reprints and permissions information is available at www.nature.com/reprints.

Correspondence and requests for materials should be addressed to A.M.C.

Publisher's note: Springer Nature remains neutral with regard to jurisdictional claims in published maps and institutional affiliations.

Methods

Cell lines. Cell lines were purchased from the American Type Culture Collection (ATCC) and maintained using standard media and conditions. All cell lines were genotyped by DNA fingerprinting analysis and tested for mycoplasma infection every 2 weeks. All cell lines used in this study were mycoplasma negative. For androgen stimulation experiments, VCaP and LNCaP cells were grown in medium supplemented with charcoal-stripped serum for 48 h and then stimulated with 10 nM DHT (Sigma-Aldrich) for 6 or 24 h.

RNA-seq. Total RNA was extracted from LNCaP and VCaP cells following DHT treatment, using the miRNeasy kit (Qiagen). RNA quality was assessed using an Agilent Bioanalyzer. Each sample was sequenced using the Illumina HiSeq 2000 (with a 100-nt read length) according to published protocols[52].

RNA-seq data analysis to identify AR-regulated genes. RNA-seq data were analyzed as previously described[53]. Briefly, the strand-specific paired-end reads were inspected for sequencing and data quality (for example, insert size, sequencing adaptor contamination, rRNA content, sequencing error rate). Libraries passing quality control were trimmed of sequencing adaptors and aligned to the human reference genome, GRCh38. Expression was quantified at the gene level using the 'intersection non-empty' mode[54] as implemented in featureCounts[55] using the Gencode v22[56] and/or MiTranscriptome[10] assemblies. All pairwise differential expression analyses were carried out using the voom–limma approach[57,58] with all default parameters. Relative expression levels (FPKM) were normalized for differences in sequencing depth using scaling factors obtained from the calcNormFactors (default parameters) function from edgeR[59].

ARGs were identified from expression data for VCaP and LNCaP cells treated with DHT for 6 and 24 h using three linear models: separate models for each of the cell lines treating the two time points as biological replicates and a merged model with all treated samples as replicates. ARGs were defined as genes that were significant (P value < 0.1 and absolute log fold change > 2) in both separate models and/or the merged model.

Identification of prostate cancer–associated protein-coding genes and lncRNAs. Raw RNA-seq data for patients with primary and metastatic prostate cancer were obtained from the TCGA/PRAD and PCF/SU2C projects, respectively. External transcriptome samples were reanalyzed using in-house pipelines (see above) to facilitate direct comparisons of expression levels and identification of differentially expressed genes. Pan-cancer analyses based on the MiTranscriptome assembly[10] were leveraged as FPKMs, and enrichment scores (SSEA) were computed as part of that project. Tissue lineage (prostate) and prostate cancer–specific genes were identified using the SSEA method as previously described[10]. Briefly, the SSEA test was used to determine whether each gene was significantly associated with a set of samples (for example, prostate cancer) or cancer progression in a given lineage (for example, prostate normal to prostate cancer). The genes were ranked according to their strength of association.

Oncomine concept analysis of the ARLNC1 signature. Genes with expression levels significantly correlated with ARLNC1 were separated into positively and negatively correlated gene lists. These two lists were then imported into Oncomine as custom concepts and queried for association with other prostate cancer concepts housed in Oncomine. All of the prostate cancer concepts with odds ratio > 2.0 and P value < 1×10^{-4} were selected. Top concepts (based on odds ratios) were selected for representation. We exported these results as the nodes and edges of a concept association network and visualized the network using Cytoscape version 3.3.0. Node positions were computed using the edge-weighted force-directed layout in Cytoscape using the odds ratio as the edge weight. Node positions were subtly altered manually to enable better visualization of Mode labels[60].

ChIP–seq data analysis. ChIP–seq data from published external and in-house datasets, GSE56288 and GSE55064, were reanalyzed using a standard pipeline. Briefly, groomed reads (vendor quality control, adaptor removal) were aligned to the GRCh38 reference genome using STAR settings that disable spliced alignment: outFilterMismatchNoverLmax: 0.05, outFilterMatchNmin: 16, outFilterScoreMinOverLread: 0, outFilterMatchNminOverLread: 0, alignIntronMax: 1. Improperly paired alignments and non-primary alignments were discarded. Peaks were called using MACS2 (callpeak --broad --qvalue 0.05 --broad-cutoff 0.05 and callpeak --call-summits --qvalue 0.05)[61] and Q (-n 100000)[62]. ChIP enrichment plots were computed from alignment coverage files (BigWig[63]) as trimmed (trim = 0.05) smooth splines (spar = 0.05). The baseline (non-specific) ChIP signal was estimated from genomic windows furthest from the center of the queried region (peak summit, TSS) and subtracted from each signal before plotting.

AR binding motif search. An unsupervised motif search was carried out using MEME[64]. DNA sequences (GRCh38) from the uni-peak ChIP–seq regions overlapping promoters (5 kb upstream, 1 kb downstream of the assembled or known TSS) of ARGs were used as input to MEME (default parameters).

ChIP–qPCR assays. AR, FOXA1 or NKX3-1 ChIP was performed following our previous protocol[32]. (Antibodies: AR, Millipore cat. no. 06-680; FOXA1, Thermo Fisher cat. no. PA5-27157; NKX3-1, CST cat. no. 83700S.) qPCR analysis was performed using the primers listed in Supplementary Table 3. Primers targeting the *CYP2B7* promoter were purchased from CST (cat. no. 84846).

RNA ISH on tissue microarray. ISH assays were performed on tissue microarray sections from Advanced Cell Diagnostics as described previously[7]. In total, 133 tissue samples were included (11 from benign prostate, 85 from localized prostate cancer and 37 from metastatic prostate cancer). ARLNC1 ISH signals were examined in morphologically intact cells and scored manually by a study pathologist, using a previously described expression value scoring system[65]. For each tissue sample, the ARLNC1 product score was averaged across evaluable tissue microarray cores. Mean ARLNC1 product scores are plotted in Fig. 2e.

RACE. 5′ and 3′ RACE were performed to determine the transcriptional start and termination sites of *ARLNC1*, using the GeneRacer RLM-RACE kit (Invitrogen), according to the manufacturer's instructions.

Northern blot analysis. The NorthernMax-Gly Kit (Ambion) was used for ARLNC1 detection following the manufacturer's protocol. Briefly, 20 µg of total RNA was resolved on a 1% agarose glyoxal gel and then transferred to nylon membrane (Roche), cross-linked to the membrane (UV Stratalinker 1800; Stratagene) and the membrane was prehybridized. Overnight hybridization was performed with an ARLNC1-specific ^{32}P-labeled RNA probe. Membranes were exposed to HyBlot CL autoradiography film (Denville Scientific). The primer sequences used for generating the probes are given in Supplementary Table 3.

RNA isolation and cDNA synthesis. Total RNA from cell lines was isolated using QIAzol Lysis reagent (Qiagen) and the miRNeasy kit (Qiagen) with DNase digestion according to the manufacturer's instructions. cDNA was synthesized using Superscript III (Invitrogen) and random primers (Invitrogen).

qRT–PCR analysis. Relative RNA levels determined by qRT–PCR were measured on an Applied Biosystems 7900HT Real-Time PCR System, using Power SYBR Green MasterMix (Applied Biosystems). All primers were obtained from Integrated DNA Technologies, and gene-specific sequences are listed in Supplementary Table 3. *GAPDH*, *HMBS* or *ACTB* was used as an internal control for quantification of gene targets. The relative expression of RNAs was calculated using the ΔΔCt method.

Cytoplasmic and nuclear RNA purification. Cell fractionation was performed using the NE-PER nuclear extraction kit (Thermo Scientific) according to the manufacturer's instructions. RNA was extracted using the previously mentioned protocol.

siRNA-mediated knockdown. siRNA oligonucleotides targeting *ARLNC1*, *AR*, *FOXA1*, *BRD4*, *NKX3-1*, *LSD1*, *IRF1*, *POU1F1* or *EZH2* and a non-targeting siRNA were purchased from Dharmacon. (si-*AR*-pool, cat. no. L-003400-00-0005; si-*FOXA1*, cat. no. LU-010319-00-0005; si-*BRD4*, cat. no. LU-004937-00-0002; si-*NKX3-1*, cat. no. LU-015422-00-0005; si-*LSD1*, cat. no. LU-009223-00-0002; si-*IRF1*, cat. no. LU-011704-00-0005; si-*POU1F1*, cat. no. LU-012546-00-0005; si-*EZH2*, cat. no. L-004218-00-0005; si-NT, cat. no. D-001810-01-05.) siRNA sequences for *ARLNC1* knockdown are listed in Supplementary Table 3. For *AR* knockdown, two more siRNAs were purchased from Life Technologies (no. HSS179972 and no. HSS179973). Transfections with siRNA (50 nM) were performed with Lipofectamine RNAiMAX according to the manufacturer's instructions. RNA and protein were harvested for analysis 72 h after transfection.

ASO-mediated knockdown. ASOs targeting *ARLNC1* were obtained from Ionis Pharmaceuticals. Transfections with ASOs (50 nM) were performed with Lipofectamine RNAiMAX according to the manufacturer's instructions. RNA and protein were harvested for analysis 72 h after transfection.

Gene expression profiling. Total RNA was extracted following the aforementioned protocol. RNA integrity was assessed using an Agilent Bioanalyzer. Microarray analysis was carried out on the Agilent Whole Human Oligo Microarray platform, according to the manufacturer's protocol. siRNA-mediated knockdown experiments were run in triplicate, comparing knockdown samples treated with two independent *ARLNC1* siRNAs to samples treated with non-targeting control siRNA. ASO-mediated knockdown experiments were run in replicate, comparing knockdown samples treated with two *ARLNC1* ASOs to samples treated with non-targeting control. An AR signature was generated using MDA-PCa-2b cells treated with 10 nM DHT in triplicate.

Analysis of Agilent 44k microarrays was carried out using limma and included background subtraction (bc.method = 'half', offset = 100) and within-array normalization (method = 'loess'). Between-array quantile normalization of average expression levels (but not log-transformed fold change) was performed using the function normalizeBetweenArrays (method = 'Aquantile'). Control probes and

probes with missing values were excluded from further analyses. Probes were annotated to Gencode v22 genes using the mapping downloaded from Ensembl (efg_agilent_wholegenome_4×44k_v2). Probes originally annotated as AK093002 were used to detect ARLNC1. Differentially expressed genes following *ARLNC1* knockdown in MDA-PCA-2b cells were identified from triplicate biological repeats using adjusted P value < 0.1 and absolute log fold change > 0.6 cutoffs. Consensus targets of *ARLNC1* knockdown using siRNA and ASOs were identified using a merged linear model (all ten samples treated as replicates) and a P value < 0.001 cutoff.

GSEA. Enrichment analyses for custom and experimentally derived signatures (that is, AR targets, genes upregulated and downregulated following DHT treatment) were carried out using the non-parametric GSEA software with all default settings. For GO term enrichment, we applied the parametric randomSet[66] enrichment statistic to voom–limma-estimated fold changes (see above).

Overexpression of ARLNC1. Full-length ARLNC1 was amplified from MDA-PCa-2b cells and cloned into the pCDH clone and expression vector (System Biosciences). Insert sequences were validated by Sanger sequencing at the University of Michigan Sequencing Core. The full-length sequence for ARLNC1 expression is listed in Supplementary Table 4.

smFISH. smFISH and image analysis were performed as described previously[67,68]. Probe sequences targeting ARLNC1, PCAT1, DANCR, *AR*, *EZH2* and *FOXA1* were designed using the probe design software at https://www.biosearchtech.com/stellaris-designer and are listed in Supplementary Table 5. TERRA probes were designed as described previously[69]. Other probes were purchased directly from LGC-Biosearch. U2OS cells were seeded in six-well dishes and transfected with ARLNC1-expression vector alone or in combination with AR expression vector, using Fugene-HD (Promega) according to the manufacturer's protocol. Cells were incubated for 24 h, reseeded into eight-well chambered coverglasses, and fixed in formaldehyde for smFISH (as described above) after 24 h.

RNA in vitro transcription. Linearized DNA templates for full-length ARLNC1, ARLNC1 fragments, ARLNC1 deletion, antisense ARLNC1, LacZ, SChLAP1-AS, THOR and AR-3′ UTR–1–980 were synthesized using T7-containing primers. In vitro transcription assays were performed with T7 RNA polymerase (Promega) according to the manufacturer's instructions. For BrU-labeled RNA synthesis, 5-bromo-UTP was added to the transcription mix. At the end of transcription, DNA templates were removed by Turbo DNase (Thermo Fisher), and RNA was recovered using the RNA Clean and Concentrator Kit (Promega). RNA size and quality were further confirmed by Agilent Bioanalyzer.

RNA–RNA in vitro interaction assays. Twenty-five microlitres of Protein A/G Magnetic Beads (Pierce) was washed twice with RIP wash buffer (Millipore, cat. no. CS203177) before incubating with BrU antibody for 1 h at room temperature. After antibody conjugation, beads were washed twice with RIP wash buffer and then resuspended in incubation buffer containing RIP wash buffer, 17.5 mM EDTA (Millipore, cat. no. CS203175) and RNase Inhibitor (Millipore, cat. no. CS203219). Equal amounts (5 pmol) of BrU-labeled RNAs (ARLNC1, ARLNC1-AS, ARLNC1-1–1300, ARLNC1-1301–2786, ARLNC1-1–700, ARLNC1-701–1300, ARLNC1-del-701–1300, *LacZ*, SChLAP1-AS, THOR) were incubated with beads in Incubation Buffer for 2 h at 4 °C. Following incubation, 2.5 pmol of the *AR* 3′ UTR–1–980 RNA fragment was added into individual tubes and incubated overnight at 4 °C. After incubation, beads were washed six times with RIP Wash Buffer. To recover RNA, beads were digested with proteinase K buffer containing RIP Wash Buffer, 1% SDS (Millipore, cat. no. CS203174) and 1.2 µg/µl proteinase K (Millipore, cat. no. CS203218) at 55 °C for 30 min with shaking. After digestion, RNA was extracted from supernatant using the miRNeasy kit (Qiagen), and reverse transcription was performed using the Superscript III system (Invitrogen). The amount of *AR* 3′ UTR–1–980 recovered in each interaction assay was quantified by qPCR analysis. Data were normalized to the ARLNC1-AS control, using the ΔCt method. We designed ASOs blocking the *AR*–ARLNC1 interaction site (ASO-blocking, Ionis Pharmaceuticals) and used them in the in vitro interaction assays. Data were normalized to the control ASO, using the ΔCt method.

RNA stability assays. LNCaP cells were treated with 5 µg/ml actinomycin D for various times as indicated. RNA was extracted and qRT–PCR was carried out as described above. RNA half-life ($t_{1/2}$) was calculated by linear regression analysis.

Cell proliferation assays. Cells treated with siRNAs or ASOs were seeded into 24-well plates and allowed to attach. Cell proliferation was recorded by IncuCyte live-cell imaging system (Essen Biosciences), following the manufacturer's instructions.

Apoptosis analysis. Cells were grown in six-well plates and transfected with nonspecific siRNA or siRNAs targeting *ARLNC1*. Apoptosis analysis was performed 48 h after transfection, using the Dead Cell Apoptosis Kit (Molecular Probes no. V13241) according to the manufacturer's instructions.

Immunoblot analysis. Cells were lysed in RIPA lysis and extraction buffer (Thermo Scientific no. 89900) supplemented with protease inhibitor cocktail (Roche no. 11836170001). Protein concentrations were quantified using the DC protein assay (Bio-Rad), and protein lysates were boiled in sample buffer. Protein extracts were then loaded and separated on SDS–PAGE gels. Blotting analysis was performed with standard protocols using polyvinylidene difluoride membrane (GE Healthcare). Membranes were blocked for 60 min in blocking buffer (5% milk in a solution of 0.1% Tween-20 in Tris-buffered saline (TBS-T)) and then incubated overnight at 4 °C with primary antibody. After three washes with TBS-T, membranes were incubated with horseradish peroxidase (HRP)-conjugated secondary antibody. Signals were visualized with an enhanced chemiluminescence system as described by the manufacturer (Thermo Scientific Pierce ECL Western Blotting Substrate). Primary antibodies used were as follows: androgen receptor (1:1,000 dilution, Millipore, no. 06-680, rabbit), GAPDH (1:5,000 dilution, Cell Signaling, no. 3683, rabbit), PSA (KLK3) (1:5,000 dilution, Dako, no. A0562, rabbit) and cleaved PARP (1:1,000 dilution, Cell Signaling, no. 9542, rabbit).

Androgen receptor reporter gene assays. Dual-luciferase reporter assays were performed using the Cignal Androgen Receptor Reporter Kit (Qiagen) according to the manufacturer's instructions. Briefly, cells were cotransfected with siRNAs (nonspecific, targeting *AR* or *ARLNC1*) and reporter vectors (negative control or AR reporter), using Lipofectamine 2000 transfection reagent (Thermo Fisher Scientific). Forty hours after transfection, DHT (or ethanol vehicle control) was added to induce AR signaling. The Dual-Luciferase assay was conducted 8 h after DHT stimulation, using the Dual-Luciferase Reporter Assay System from Promega (cat no. 1910). Reporter activity was analyzed on the basis of the ratio of firefly/*Renilla* activity to normalize for cell number and transfection efficiency.

In vivo experiments. All experiments were approved by the University of Michigan Institutional Animal Care and Use Committee. For tumor generation with shRNA-mediated knockdown, shRNA targeting *ARLNC1* was cloned into pSIH1-H1-copGFP-T2A-Puro (System Biosciences). Lentiviral particles were generated at the University of Michigan Vector Core. LNCaP-AR cells were infected with lentivirus expressing *ARLNC1* shRNA for 48 h. Knockdown of ARLNC1 was confirmed by qPCR analysis. Male athymic nude mice were randomized into two groups at 6 to 8 weeks of age. Five million cells expressing sh-*ARLNC1* or sh-vector were injected into bilateral flanks of mice. Caliper measurements were taken in two dimensions twice a week by an investigator blinded to the study objective and used to calculate tumor volume. The study was terminated when the tumor volume reached 1,000 mm^3. For ASO treatment in vivo, 6- to 8-week-old male athymic nude mice were inoculated subcutaneously with MDA-PCa-2b cells suspended in a Matrigel scaffold in the posterior dorsal flank region (5 million cells per site, two sites per animal). When the mean tumor volume reached approximately 150 mm^3, mice were randomized into two groups and treated with *ARLNC1*-specific or control ASO. ASOs, dosed at 50 mg per kg body weight, were subcutaneously injected between the scapulae once daily for three periods of 5 d on/2 d off. Tumor size was measured twice per week using a digital caliper by a researcher blinded to the study design. Mouse body weights were monitored throughout the dosing period. When the average tumor size in the control group reached 1,500 mm^3, mice were euthanized and the primary tumors were excised for weight determination. One-third of the resected specimen was placed in 10% formalin buffer, and the remaining tissue was snap-frozen.

BrU-seq and BrUChase-seq. BrU-seq and BrUChase-seq assays were performed as previously described[70,71] with MDA-PCa-2b cells treated with either si-NT or si-*ARLNC1*. BrU labeling was performed for 30 min, and chase experiments were performed for 6 h.

Statistical analysis. For in vivo experiments, power analysis (GPOWER software) performed for each tumor type tested to date indicates that the sample size we chose yields a statistical power >90% for detection of tumor size reduction of 40%. Sample sizes were not predetermined for all other assays. For in vivo experiments, animals were randomized. Randomization was not performed for all other assays. Statistical analyses were performed using GraphPad Prism software or using R. Data are presented as either means ± s.e.m. or means ± s.d. All of the experiments were performed in biological triplicate unless otherwise specified. Statistical analyses shown in figures represent two-tailed t tests, one-way ANOVA, two-way ANOVA or Kruskal–Wallis rank-sum tests as indicated. $P < 0.05$ was considered to be statistically significant. Details regarding the statistical methods employed during microarray, RNA-seq and ChIP–seq data analysis were included in the aforementioned methods for bioinformatics analyses.

Reporting Summary. Further information on experimental design is available in the Nature Research Reporting Summary linked to this article.

Code availability. Software for transcriptome meta-assembly and lncRNA discovery is available at https://tacorna.github.io/.

Data availability. RNA-seq and microarray data sets generated from this study have been deposited into the Gene Expression Omnibus, with accession GSE110905. Other data supporting the findings of this study are included in the Supplementary Information.

References

52. Prensner, J. R. et al. Transcriptome sequencing across a prostate cancer cohort identifies PCAT-1, an unannotated lincRNA implicated in disease progression. *Nat. Biotechnol.* **29**, 742–749 (2011).
53. Cieslik, M. et al. The use of exome capture RNA-seq for highly degraded RNA with application to clinical cancer sequencing. *Genome Res.* **25**, 1372–1381 (2015).
54. Anders, S., Pyl, P. T. & Huber, W. HTSeq-a Python framework to work with high-throughput sequencing data. *Bioinformatics* **31**, 166–169 (2015).
55. Liao, Y., Smyth, G. K. & Shi, W. featureCounts: an efficient general purpose program for assigning sequence reads to genomic features. *Bioinformatics* **30**, 923–930 (2014).
56. Harrow, J. et al. GENCODE: the reference human genome annotation for The ENCODE Project. *Genome Res.* **22**, 1760–1774 (2012).
57. Law, C. W., Chen, Y., Shi, W. & Smyth, G. K. voom: precision weights unlock linear model analysis tools for RNA-seq read counts. *Genome Biol.* **15**, R29 (2014).
58. Ritchie, M. E. et al. limma powers differential expression analyses for RNA-sequencing and microarray studies. *Nucleic Acids Res.* **43**, e47 (2015).
59. Robinson, M. D., McCarthy, D. J. & Smyth, G. K. edgeR: a Bioconductor package for differential expression analysis of digital gene expression data. *Bioinformatics* **26**, 139–140 (2010).
60. Cline, M. S. et al. Integration of biological networks and gene expression data using Cytoscape. *Nat. Protoc.* **2**, 2366–2382 (2007).
61. Zhang, Y. et al. Model-based analysis of ChIP-Seq (MACS). *Genome Biol.* **9**, R137 (2008).
62. Hansen, P. et al. Saturation analysis of ChIP-seq data for reproducible identification of binding peaks. *Genome Res.* **25**, 1391–1400 (2015).
63. Kent, W. J., Zweig, A. S., Barber, G., Hinrichs, A. S. & Karolchik, D. BigWig and BigBed: enabling browsing of large distributed datasets. *Bioinformatics* **26**, 2204–2207 (2010).
64. Bailey, T. L. et al. MEME SUITE: tools for motif discovery and searching. *Nucleic Acids Res.* **37**, W202–W208 (2009).
65. Mehra, R. et al. A novel RNA in situ hybridization assay for the long noncoding RNA SChLAP1 predicts poor clinical outcome after radical prostatectomy in clinically localized prostate cancer. *Neoplasia* **16**, 1121–1127 (2014).
66. Newton, M. A., Quintana, F. A., Den Boon, J. A., Sengupta, S. & Ahlquist, P. Random-set methods identify distinct aspects of the enrichment signal in gene-set analysis. *Ann. Appl. Stat.* **1**, 85–106 (2007).
67. Raj, A., van den Bogaard, P., Rifkin, S. A., van Oudenaarden, A. & Tyagi, S. Imaging individual mRNA molecules using multiple singly labeled probes. *Nat. Methods* **5**, 877–879 (2008).
68. Niknafs, Y. S. et al. The lncRNA landscape of breast cancer reveals a role for DSCAM-AS1 in breast cancer progression. *Nat. Commun.* **7**, 12791 (2016).
69. Rossiello, F. et al. DNA damage response inhibition at dysfunctional telomeres by modulation of telomeric DNA damage response RNAs. *Nat. Commun.* **8**, 13980 (2017).
70. Paulsen, M. T. et al. Coordinated regulation of synthesis and stability of RNA during the acute TNF-induced proinflammatory response. *Proc. Natl Acad. Sci. USA* **110**, 2240–2245 (2013).
71. Paulsen, M. T. et al. Use of Bru-Seq and BruChase-Seq for genome-wide assessment of the synthesis and stability of RNA. *Methods* **67**, 45–54 (2014).

nature research

Corresponding author(s): Arul M. Chinnaiyan

Reporting Summary

Nature Research wishes to improve the reproducibility of the work that we publish. This form provides structure for consistency and transparency in reporting. For further information on Nature Research policies, see Authors & Referees and the Editorial Policy Checklist.

Statistical parameters

When statistical analyses are reported, confirm that the following items are present in the relevant location (e.g. figure legend, table legend, main text, or Methods section).

n/a	Confirmed	
☐	☒	The exact sample size (*n*) for each experimental group/condition, given as a discrete number and unit of measurement
☐	☒	An indication of whether measurements were taken from distinct samples or whether the same sample was measured repeatedly
☐	☒	The statistical test(s) used AND whether they are one- or two-sided *Only common tests should be described solely by name; describe more complex techniques in the Methods section.*
☐	☒	A description of all covariates tested
☐	☒	A description of any assumptions or corrections, such as tests of normality and adjustment for multiple comparisons
☐	☒	A full description of the statistics including central tendency (e.g. means) or other basic estimates (e.g. regression coefficient) AND variation (e.g. standard deviation) or associated estimates of uncertainty (e.g. confidence intervals)
☐	☒	For null hypothesis testing, the test statistic (e.g. *F*, *t*, *r*) with confidence intervals, effect sizes, degrees of freedom and *P* value noted *Give P values as exact values whenever suitable.*
☒	☐	For Bayesian analysis, information on the choice of priors and Markov chain Monte Carlo settings
☒	☐	For hierarchical and complex designs, identification of the appropriate level for tests and full reporting of outcomes
☐	☒	Estimates of effect sizes (e.g. Cohen's *d*, Pearson's *r*), indicating how they were calculated
☐	☒	Clearly defined error bars *State explicitly what error bars represent (e.g. SD, SE, CI)*

Our web collection on statistics for biologists may be useful.

Software and code

Policy information about availability of computer code

Data collection	RNA seq, Microarray and qRT-PCR data were collected using vendor's software on Illumina HiSeq 2000, Agilent Whole Human Oligo Microarray, Applied Biosystems 7900HT Real-Time PCR platforms respectively. Microscopy images were acquired using Metamorph.
Data analysis	Software for transcriptome meta-assembly and lncRNAs discovery is available at https://tacorna.github.io/. Gene signatures were obtained using GSEA software. Image analysis was performed using custom-written macros in Image J and can be shared upon request. Statistical analysis was performed using Graphpad-Prism 6.0 and R.

For manuscripts utilizing custom algorithms or software that are central to the research but not yet described in published literature, software must be made available to editors/reviewers upon request. We strongly encourage code deposition in a community repository (e.g. GitHub). See the Nature Research guidelines for submitting code & software for further information.

Data

Policy information about availability of data

All manuscripts must include a data availability statement. This statement should provide the following information, where applicable:

- Accession codes, unique identifiers, or web links for publicly available datasets
- A list of figures that have associated raw data
- A description of any restrictions on data availability

RNA-seq and microarray datasets generated from this study have been deposited into Gene Expression Omnibus, with accession number: GSE110905. Other data supporting the finding of this study are included in the Supplementary Information files. Software for transcriptome meta-assembly and lncRNAs discovery is available at https://tacorna.github.io/. We have no restrictions on data availability and data can be shared upon request.

Field-specific reporting

Please select the best fit for your research. If you are not sure, read the appropriate sections before making your selection.

☒ Life sciences ☐ Behavioural & social sciences

For a reference copy of the document with all sections, see nature.com/authors/policies/ReportingSummary-flat.pdf

Life sciences

Study design

All studies must disclose on these points even when the disclosure is negative.

Sample size	For in vivo experiments, power analysis (GPOWER software) performed for each tumor type tested to date indicates this animal number yields a statistical power >90% for detection of tumor size reduction of 40%. Sample sizes were not pre-determined for all other assays.
Data exclusions	No data were excluded.
Replication	All experiments were carried out at least 3 independent times for statistical reproducibility, unless otherwise stated, as represented by p-values.
Randomization	For in vivo experiments, animals were randomized. Randomization was not performed for all other assays.
Blinding	For in vivo experiments, tumor size was measured twice per week using a digital caliper by a researcher blinded to the study design. Blinding was not performed for all other assays.

Materials & experimental systems

Policy information about availability of materials

n/a	Involved in the study
☒	☐ Unique materials
☐	☒ Antibodies
☐	☒ Eukaryotic cell lines
☐	☒ Research animals
☒	☐ Human research participants

Antibodies

Antibodies used	Primary antibodies used in this study were: Androgen Receptor (1:1000 dilution, Millipore, #06-680, rabbit), GAPDH (1:5000 dilution, Cell Signaling, #3683, rabbit), PSA (1:5000 dilution, Dako, #A0562, rabbit), FOXA1 (Thermo Fisher Cat# PA5-27157) NKX3.1 (CST Cat# 83700S) and cleaved PARP (1:1000 dilution, Cell Signaling, #9542, rabbit).
Validation	All antibodies were validated by the vendors. Androgen receptor and PSA antibodies were also validated by siRNA treatment and androgen signaling assays respectively.

Eukaryotic cell lines

Policy information about cell lines

Cell line source(s)	All cell lines were purchased form ATCC.
Authentication	All cell lines were genotyped by STR profiling in house based on ATCC markers.

Mycoplasma contamination	All cells were tested for mycoplasma every two weeks.
Commonly misidentified lines (See ICLAC register)	Study does not include misidentified lines.

Research animals

Policy information about studies involving animals; ARRIVE guidelines recommended for reporting animal research

Animals/animal-derived materials	Male athymic nude mice were used in our in vivo studies.

Method-specific reporting

n/a	Involved in the study
☒	☐ ChIP-seq
☒	☐ Flow cytometry
☒	☐ Magnetic resonance imaging